Applied Thermal Engineering 280 (2025) 128315

Contents lists available at ScienceDirect

Applied Thermal Engineering

journal homepage: www.elsevier.com/locate/apthermeng

Research Paper

Condensation of high-concentration NH_3/H_2O in plate heat exchangers: A combined model

Xuan Tao [a,c,*], Yunwei Shen [a], Haoren Wang [a,b,**], Bo Wang [a], Carlos A. Infante Ferreira [c]

[a] Cryogenic Center, Hangzhou City University, Hangzhou 310015, China
[b] Key Laboratory of Refrigeration and Cryogenic Technology of Zhejiang Province, Zhejiang University, Hangzhou 310027, China
[c] Process and Energy Laboratory, Delft University of Technology, Leeghwaterstraat 39, 2628 CB Delft, the Netherlands

ARTICLE INFO

Keywords:
Equilibrium model
Non-equilibrium model
Temperature glide
Concentration gradient
Condensation mechanism
Two-phase pressure drop

ABSTRACT

NH_3/H_2O based systems are promising for thermal energy storage and thermal energy conversion. These systems are used for absorption energy storage and Kalina cycles. This paper investigates the condensation of high-concentration NH_3/H_2O in vertically downward plate heat exchangers. A combined method is proposed by discussing the applicability of equilibrium and non-equilibrium models. Both models are necessary for zeotropic mixtures with large temperature glide. The non-equilibrium model applies where the temperature glide is non-linear or the vapor is in non-equilibrium with the liquid. The equilibrium model becomes applicable with decreasing vapor qualities. Heat transfer correlations are proposed according to the equilibrium model, which interpret convective condensation and gravity-controlled condensation. The additional heat transfer resistance is calculated considering mass transfer. The non-equilibrium model is further developed quantifying the heat and mass transfer of vapor and neglecting the mass transfer resistance of the liquid. The non-equilibrium model transforms into the equilibrium model as the concentration gradient of vapor approaches zero. Additionally, a frictional pressure drop model for separated flow conditions is proposed and quantifies the two-phase shear force.

1. Introduction

The present environmental problems drive the mitigation of carbon emissions. Fossil fuels are being replaced by renewable resources [46]. The recovery of low-grade heat plays a growing role in reducing energy consumption [26]. NH_3 has emerged as a promising carrier for energy storage because of the high volumetric energy density in power transmission systems. As a zero-carbon fuel and hydrogen carrier, NH_3 enables efficient long-term and large-scale energy storage for intermittent renewable energy sources like wind and solar. NH_3/H_2O is a by-product in the chemical engineering industry, and can be purified to produce pure NH_3 [27].

NH_3/H_2O is a well-recognized working fluid in energy storage, refrigeration, and power plants [14,49]. High-concentration NH_3/H_2O is the working fluid of the Kalina cycle, with condensation or absorption being the key process[18,32]. Plate heat exchangers (PHEs) are widely used in NH_3/H_2O systems with the advantage of a small working fluid charge and superior heat transfer performance, so that the size of the system is reduced[35].

1.1. The heat and mass transfer of NH_3/H_2O condensation

NH_3/H_2O is a zeotropic mixture with large temperature glide. Fig. 1 (a) shows the equilibrium temperature for high mass concentrations (*MCs*), which can be divided into an approximately-linear temperature glide region for low vapor qualities and a non-linear temperature glide region for high vapor qualities. In the former region, the equilibrium temperature increases approximately linearly with vapor qualities, while the temperature glide changes sharply in the latter region. dT/dh is the derivative of the equilibrium temperature with the two-phase enthalpy at a constant pressure and bulk concentration. dT/dh is used to indicate the mass transfer resistance, and is given in Fig. 1(b). The integral of the value, $\int dT/\int dh$, in the two-phase region gives $\Delta T_{LV}/\Delta h_{LV}$. $\Delta T_{LV}/\Delta h_{LV}$ is equal to dT/dh only if dT/dh is constant [12]. In the approximately-linear temperature glide region, dT/dh increases smoothly with mass concentration and vapor qualities. The change is irregular in the non-linear temperature glide region.

* Corresponding author at: Cryogenic Center, Hangzhou City University, Hangzhou 310015, China.
** Corresponding author at: Key Laboratory of Refrigeration and Cryogenic Technology of Zhejiang Province, Zhejiang University, Hangzhou 310027, China.
E-mail addresses: taox@hzcu.edu.cn (X. Tao), wang_haoren@zju.edu.cn (H. Wang).

https://doi.org/10.1016/j.applthermaleng.2025.128315
Received 18 June 2025; Received in revised form 25 August 2025; Accepted 9 September 2025
Available online 10 September 2025

Nomenclature

Symbols

A	Actual heat transfer area [m^2]
Co	Convection number [-]
c_p	Specific heat capacity [$Jkg^{-1}K^{-1}$]
C_v	Vapor density in mole base [mol m^{-3}]
d_g	Channel gap [mm]
d_h	Hydraulic diameter [mm]
d_p	Plate thickness [mm]
D_v	Vapor diffusion coefficient [m^2s^{-1}]
f	Darcy friction factor [-]
F	Mass transfer coefficient [kmol $m^{-2}s^{-1}$]
Fr	Froude number [-]
g	Gravitational constant [ms^{-2}]
G	Mass flux [$kgm^{-2}s^{-1}$]
h	Enthalpy [Jkg^{-1}]
L	Non-dimensional length [-]
Le	Lewis number [-]
L_p	Port-to-port plate length [mm]
M	Mole mass [kg $kmol^{-1}$]
$\dot{m}$“	Condensing flux [$kgm^{-2}s^{-1}$]
$\dot{m}$	Mass flow rate [kgs^{-1}]
MC	Mass concentration of NH_3 [-]
N	Condensing flux in mole base [kmol $m^{-2}s^{-1}$]
Nu	Nusselt number [-]
P	Pressure [kPa]
Pr	Prandtl number [-]
$\dot{Q}$	Heat flow rate [W]
Re	Reynolds number [-]
Sc	Schmidt number [-]
Sh	Sherwood number [-]
T	Temperature [℃]
v	Superficial velocity [ms^{-1}]
We	Weber number [-]
W_p	In gasket plate width [mm]
x	Vapor quality [-]
x_L	Liquid mole concentration [-]
x_V	Vapor mole concentration [-]
z	Mole concentration of condensing flux [-]

Greek symbols

α	Heat transfer coefficient [$Wm^{-2}K^{-1}$]
β	Chevron angle to flow direction [°]
β_V	Vapor mass transfer coefficient [ms^{-1}]
Δ	Difference
Φ	Surface enlargement factor [-]
λ	Thermal conductivity [$Wm^{-1}K^{-1}$]
Λ_{wave}	Corrugation wavelength [mm]
μ	Dynamic viscosity [Pas]
ρ	Density [kgm^{-3}]
σ	Surface tension [Nm^{-1}]

Subscripts

av	Averaged
aw	Ammonia water
b	Bulk
c	Combined condensation
cc	Convective condensation
eq	In equilibrium condition
exp	Measured value
gc	Gravity-controlled condensation
i	Interface
in	Inlet
L	Liquid or liquid bulk
Li	Liquid interface
LO	Liquid only
LT1	Limit 1 in Eq. (A2)
LT2	Limit 2 in Eq. (A3)
LV	From liquid to vapor
mix	Mixture
*mix*0	Ideal mixture
out	Outlet
pure	Pure fluid
pre	Predicted value
re	Reduced pressure
sat	At saturated conditions
sub	Subcooling
sup	Superheating
T	Total
TP	Two-phase
V	Vapor or vapor bulk
Vi	Vapor interface
w	Cooling water
wall	Plate wall

Abbreviations

ALTGR	Approximately-linear temperature glide region
HTC	Heat transfer coefficient
MTC	Mass transfer coefficient
PHE	Plate heat exchanger
NLTGR	Non-linear temperature glide region
SBG	Silver-Bell-Ghaly

The condensation of NH_3/H_2O is characterized by the mass transfer of both components from vapor to liquid phase. Heat is released to a coolant flow. The process is also classified as absorption. The temperature and mass concentration at the two-phase interface are the basis to predict heat and mass transfer. The modelling approaches of zeotropic condensation are classified into conservation equation models, non-equilibrium models, equilibrium models and empirical models[15]. Non-equilibrium and equilibrium models were recommended given their balance of applicability and computational complexity [29].

1.1.1. Equilibrium model

The equilibrium model assumes that overall the vapor and liquid bulk concentrations are at equilibrium. The vapor/liquid interface concentrations are identical to the vapor/liquid bulk concentrations. The concentrations of the liquid and vapor are determined by the overall concentration, vapor quality and pressure. The interface temperature is equal to the equilibrium temperature as shown in Fig. 1(a). The liquid bulk can be subcooled, while the vapor bulk can be superheated. It is “concentration equilibrium” instead of “temperature equilibrium”. The mass transfer is considered by adding a heat transfer resistance of the vapor sensible cooling, but the mass transfer resistance is not calculated directly [4,38]. The calculation is given in Eq. (1) and is known as the Silver-Bell-Ghaly (SBG) method [4,38]. For a fixed operating pressure, dT/dh is a function of vapor qualities and mass concentrations.

$$\alpha_{c,mix} = \left(\alpha_{c,pure}^{-1} + xc_{p,V}\frac{dT}{dh}\alpha_V^{-1}\right)^{-1} \quad (1)$$

Del Col et al. [12] improved the equilibrium model by involving flow patterns. Similar to pure fluids, the condensation heat transfer

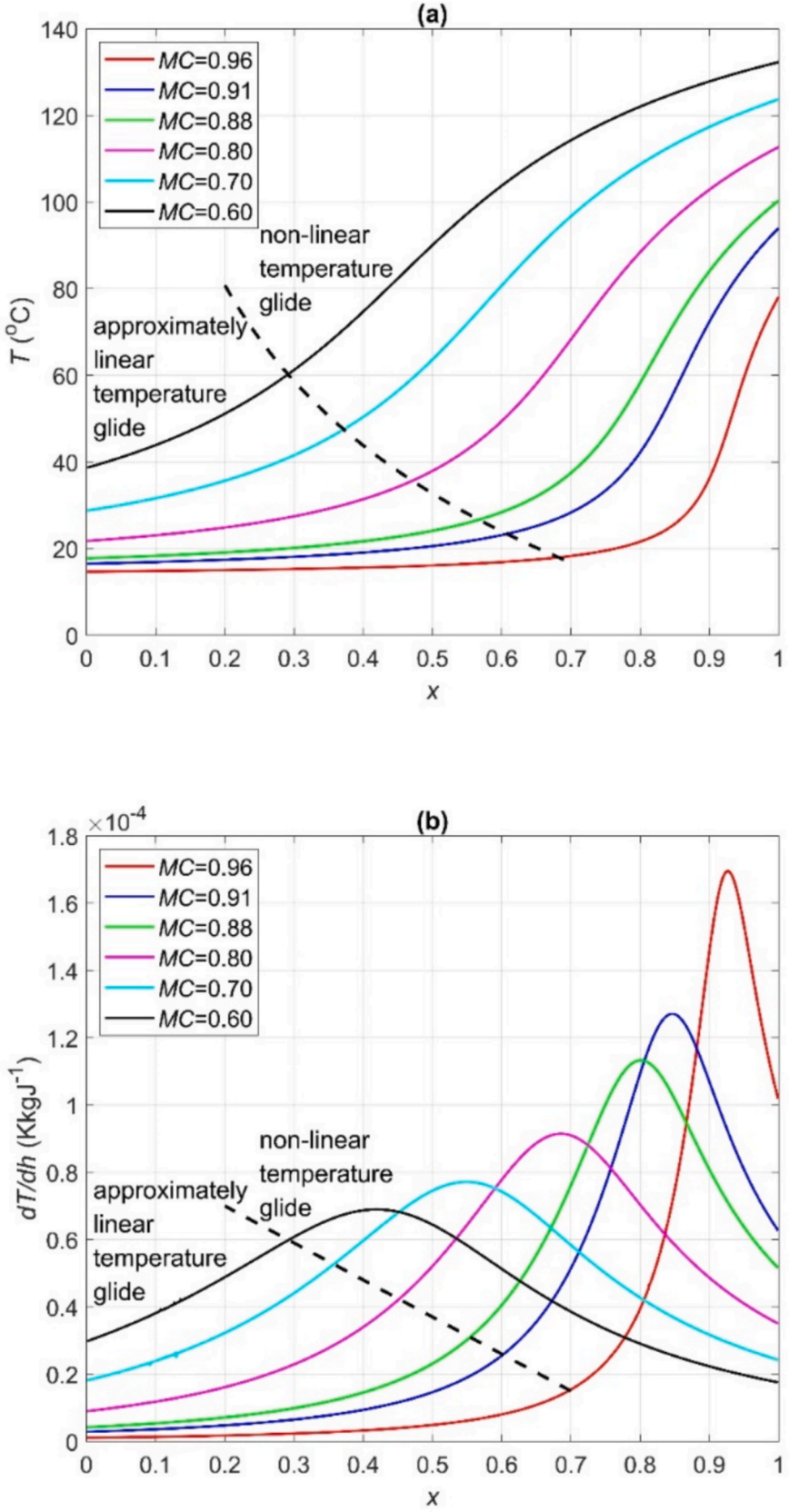

Fig. 1. (a) Equilibrium temperature and (b) dT/dh as a function of vapor quality for different mass concentrations at 690 kPa. The data are adapted from Refprop 10.0 [25].

coefficients (HTCs) of mixtures are a function of flow patterns. For annular flow, convective condensation is well predicted using the SBG method and considering the interfacial roughness. The equilibrium assumption is met because of the strong shear force and mixing. In terms of stratified flow, gravity-controlled condensation is over-predicted by the SBG method. Stratification leads to deviation from the equilibrium assumption. The deviation is larger for small mass flux and large temperature glide. When the SBG method is modified by quantifying the non-equilibrium effect, the accuracy is improved. The model is applicable for mixtures with a temperature glide of 3.5–22 K [12]. This method is also adopted by Deng et al. [13]. The interfacial shear and stratification effect are identified considering the condensation mechanisms.

1.1.2. Non-equilibrium model

According to the fundamental assumption of the non-equilibrium model, the thermodynamic equilibrium of vapor/liquid only prevails at the interface, where the concentrations are in equilibrium and the temperatures are the same. However, the vapor and liquid bulk have concentration and temperature gradients. The heat and mass transfer resistances of the vapor are assumed to be restricted to a thin film [10,33]. Mass is transferred from vapor to liquid across the interface. In Eq. (2), mass transfer was determined from the vapor to interface and from the interface to liquid with mass transfer coefficient (MTC), F. x_{Li} and x_{Vi} are the NH_3 concentrations of liquid and vapor at the interface. x_L and x_V are the concentrations of liquid bulk and vapor bulk [37]. z is the ratio of NH_3 flux to total flux and is defined in Eq. (3), where N is the condensing flux at the interface and is in the mole base [37]. Eq. (2) is the general form, which can be simplified according to the value of MTC.

$$N_{NH_3}+N_{H_2O}=\underbrace{F_V\ln\left(\frac{z-x_{Vi}}{z-x_V}\right)}_{\text{Vapor mass transfer}}=\underbrace{F_L\ln\left(\frac{z-x_L}{z-x_{Li}}\right)}_{\text{Liquid mass transfer}} \tag{2}$$

$$z=\frac{N_{NH_3}}{N_{NH_3}+N_{H_2O}} \tag{3}$$

Under the assumption that the two-phase interface is at equilibrium, Sieres and Fernández-Seara [37] distinguished between condensation and absorption by interpreting Eq. (2). The liquid bulk is not in equilibrium with the vapor bulk. Fig. 2 and Fig. 3 show the concentration and temperature profiles. $x_V \geqslant x_L$ in condensation or absorption. T_i is the interface temperature. At the system pressure, the saturated temperatures of liquid and vapor bulk, $T_{L,sat}$ and $T_{V,sat}$, are determined by the bulk concentrations of liquid and vapor, respectively. $T_{L,sat}$ and $T_{V,sat}$ differ from the real bulk temperatures, T_L and T_V. The subcooled liquid bulk and superheated vapor bulk deviate from equilibrium condition. The heat and mass transfer are driven by the temperature and concentration differences between the interface and liquid–vapor bulk.

Fig. 2(a) shows the concentration profile for $x_{Li} < z < x_V$, where $x_{Vi} > x_V$ and $x_{Li} > x_L$. Both NH_3 and H_2O flow from vapor to liquid. In this case, the process is both condensation and absorption. The interface temperature is lower than the saturation temperatures of vapor and liquid [37]. Fig. 2(b) further indicates the possible temperature profiles with subcooling and superheating, ΔT_{sub} and ΔT_{sup}. Fig. 2(b) shows $T_L < T_i < T_V$. Accordingly, heat is transferred from vapor to liquid through the interface.

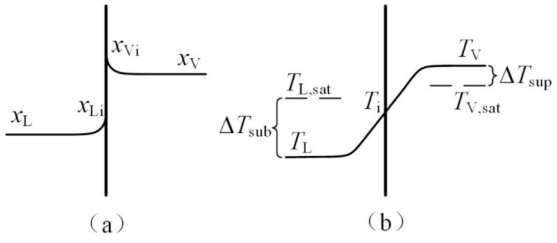

Fig. 2. Concentration and temperature profiles of NH_3/H_2O during condensation or absorption with $x_{Vi} > x_V$ and $x_{Li} > x_L$ (adapted from Sieres and Fernández-Seara [37]).

Fig. 3 is the typical condition of absorption with $x_{Vi} < x_V$ and $x_{Li} > x_L$, which is further classified according to the flow direction of H_2O. In the first case, both NH_3 and H_2O are absorbed into the liquid with $x_V < z < 1$. In the second case, NH_3 flows from vapor to liquid but H_2O is transferred in the opposite direction, with $z > 1$ or $z < 0$. The interface temperature is lower than the liquid saturation temperature and higher than the vapor saturation temperature [37]. Fig. 3(b) shows $T_L < T_i < T_V$, which is similar to Fig. 2(b). As shown in Fig. 3(c), it is possible that $T_L < T_V < T_i$ or $T_V < T_L < T_i$ [21,44]. The latent heat is released at the interface and is transferred to the liquid and vapor bulk.

The above conditions appear at different parts of a heat exchanger [21,44]. This paper does not distinguish between condensation and absorption as long as NH_3 is transferred from vapor to liquid and heat is removed by external cooling.

1.2. Previous studies on PHEs and other channels

This Section presents the previous researches on condensation or absorption in PHEs and other channels. Table 1 gives a summary of the numerical models and experimental work, which includes heat and mass transfer correlations and flow configurations. The mass concentrations of vapor and liquid are also presented. For the listed experimental researches, the temperature difference between the liquid and coolant is considered as the driving force. The total heat transfer to the coolant, $\dot{Q}_T$, is calculated using Eq. (4). α_L and α_w are the liquid and coolant HTCs, respectively. α_L is determined by the liquid temperatures at the inlet and outlet, $T_{L,in}$ and $T_{L,out}$. The heat and mass transfer between the vapor and interface are not quantified. The numerical models applied thermodynamic equilibrium at the interface and calculated the mass transfer resistances. The models of bubble mode additionally require bubble dynamics equations.

$$\dot{Q}_T=\frac{A}{\frac{1}{\alpha_L}+\frac{d_p}{\lambda_{wall}}+\frac{1}{\alpha_w}}\frac{\left(T_{L,in}-T_{w,out}\right)-\left(T_{L,out}-T_{w,in}\right)}{\ln\frac{T_{L,in}-T_{w,out}}{T_{L,out}-T_{w,in}}} \tag{4}$$

Kang et al. [21] proposed a numerical model for the coupled heat and mass transfer in a PHE operating as a bubble absorber. The NH_3/H_2O liquid flowed from the top to bottom, while the NH_3/H_2O vapor and coolant flowed upward. The mass transfer resistances of liquid and vapor were calculated. The two-phase interface was at equilibrium temperatures and concentrations. The profiles of temperatures and concentrations were predicted. The model was also extended to falling film mode with the same flow directions. The bubble mode was superior to the falling film mode in terms of the heat and mass transfer performances [22].

The model of Triché et al. [44] was similar to Kang et al. [21,22], but the liquid flowed co-currently with the vapor. The predicted heat transfer rates were slightly larger than the experimental values. The possible reason is that the wall surface was not completely wetted by the liquid film NH_3 was absorbed all over the heat exchanger. H_2O was desorbed at the inlet and was absorbed at the rest of the heat exchanger.

Lee et al. [24] experimentally compared the heat and mass transfer in a special PHE working as falling film and bubble modes. Both NH_3 vapor and cooling water were counter to the liquid flow. The MTC was calculated based on the difference between the equilibrium liquid concentration and real liquid concentration. In general, the bubble mode showed better mass transfer performance, while the falling film mode had superior heat transfer performance.

Cerezo et al. [5] experimentally studied the absorption of NH_3/H_2O in a PHE in bubble mode. NH_3 vapor was co-current with NH_3/H_2O and was not completely absorbed at the outlet. The heat and mass transfer were enhanced by lower liquid concentration, reduced cooling water

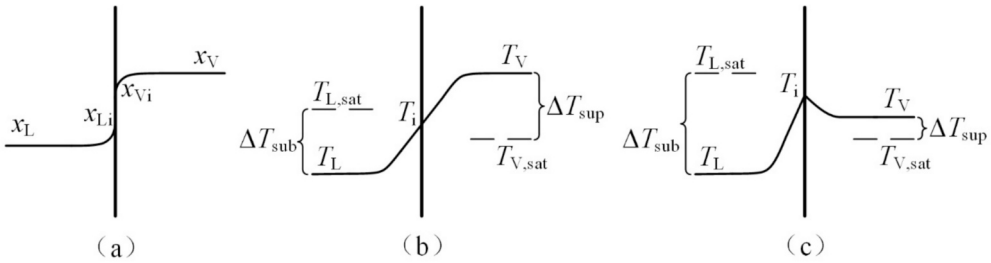

Fig. 3. Concentration and temperature profiles of NH_3/H_2O during absorption with $x_{Vi} < x_V$ and $x_{Li} > x_L$ (adapted from Sieres and Fernández-Seara [37]).

temperature and increased system pressure. Cerezo et al. [6] built a model assuming equilibrium conditions at the interface. The model was validated with experimental results.

Jung et al. [20] measured the absorption of NH_3/H_2O. The NH_3 vapor was injected in bubble mode and flowed upward. Three types of PHEs with different geometric parameters were compared. The one with a larger ratio of length to width showed better heat transfer performance.

NH_3/H_2O condensation/ absorption in other channels has also been investigated. van de Bor et al. [45] measured the absorption of NH_3/H_2O within the annulus of a mini-channel. NH_3/H_2O has a bulk mass concentration of 0.37. The HTCs increase with larger mass fluxes, vapor qualities and heat fluxes, which are noticeably over-predicted by condensation heat transfer correlations. The mass transfer resistance of the mixture significantly deteriorates the heat transfer. The frictional pressure drop is well predicted by the correlations of pure fluids.

The condensation of high-concentration NH_3/H_2O shows distinct characteristics. The concentrations of the vapor and liquid are closer to equilibrium. Fronk and Garimella [16] suggested apparent HTCs, which were calculated using the equilibrium temperature. The equilibrium model under-predicts the experimental HTCs of small tubes[17]. As shown in Fig. 1(a), high-concentration NH_3/H_2O has non-linear temperature glide in the high vapor quality region, where the interface temperature is over-predicted. A non-equilibrium model is proposed. The condensation HTCs of pure NH_3 are used to predict the liquid heat transfer considering that high-concentration NH_3/H_2O has similar fluid properties as pure NH_3. The vapor mass transfer resistance is quantified, while the liquid mass transfer resistance is neglected. This non-equilibrium model applies to annular and non-annular flow [17]. Since NH_3/H_2O has a higher saturated temperature than pure NH_3, the heat flux of NH_3/H_2O is predicted to be larger. Chandrasekaran et al. [7] measured the absorption of NH_3/H_2O in a microchannel, comparing the performance of co-current flow and counter-current flow. The overall heat transfer rates of both flow configurations are similar, while the co-current flow has larger subcooling at the outlet. The numerical model distinguishes wet regions and dry regions. The phase change takes place in the wet regions, and the dry regions are used for the sensible heat transfer of vapor [7].

Aminyavari et al [2,3] developed numerical models for co-current flow and counter-current flow in tubes. For co-current flow, the phase change mainly happens at the top of the tubes. The models were experimentally validated, showing good agreement[2]. For counter-current flow, the predicted mass transfer rates are smaller than the experimental values, indicating adiabatic absorption. Additionally, minor prediction errors are shown to result in major miscalculations of absorber size[3].

As shown in Table 1, the vapor has a high NH_3 concentration, while the liquid has a low concentration. Experimental research takes the temperature difference between the liquid and coolant as the driving force. The overall heat transfer rate is calculated without considering the proportion of latent heat and sensible heat. Because the mixture temperatures vary sharply, the corresponding heat transfer correlations are limited to the original ranges[20]. The mass transfer is analyzed by calculating the overall mass of absorbed NH_3. The numerical models assume the two-phase to be in equilibrium at the interface and solve the heat and mass transfer equations. The heat and mass transfer coefficients are determined by empirical correlations or heat and mass transfer analogies. The accuracy of the correlations is not fully analyzed. These numerical models are limited to film flow and dispersed bubble flow, and do not include other flow patterns.

The equilibrium model is straightforward but is limited to narrow ranges. The difference between interface and equilibrium conditions is neglected, which is oversimplified when the temperature glide is non-linear. The non-equilibrium model applies for general conditions, but the requirement on mass transfer relevant properties complicates the prediction. Moreover, when the vapor bulk concentration is close to the vapor interface concentration, the phase change is only driven by temperature difference. The calculation of the phase change driven by concentration difference gives zero, which deviates from the value calculated using temperature difference. And thus the non-equilibrium model becomes erratic. Yan et al. [48] proposed to approximate the concentration difference using the temperature glide. The proposed model simplifies the non-equilibrium theory with the analogy of equilibrium model. The model applies to several zeotropic mixtures with smaller temperature glide than NH_3/H_2O. Considering the sharp change of the NH_3/H_2O temperature glide shown in Fig. 1, the condensation of NH_3/H_2O should be specifically analyzed.

The condensation of NH_3/H_2O is driven by the temperature difference and concentration difference. The dominance of heat transfer or mass transfer depends on the operating conditions. Both models are necessary to cover a wide range of bulk concentrations and vapor qualities. The equilibrium model can be considered as a special condition of the non-equilibrium model with negligible mass transfer resistance [47]. The equilibrium model applies to the condensation only driven by temperature difference, where the interface concentration is identical to the overall bulk concentration. A specific procedure is needed to reduce the non-equilibrium model to the equilibrium model. This paper investigates the condensation of high-concentration NH_3/H_2O in PHEs. The slope of the temperature glide is analyzed to evaluate equilibrium and non-equilibrium models. The advantages of both models are combined by interpreting the transition from non-equilibrium to equilibrium conditions. The equilibrium condition is met for low vapor qualities as the temperature glide is close to linear. The new model reveals the relation between interface and equilibrium concentrations. The condensation mechanism is analyzed based on flow patterns. The heat transfer resistance is quantified as a function of liquid film characteristics. Additionally, a unified frictional pressure drop model is developed for pure NH_3 and high-concentration NH_3/H_2O.

2. Heat and mass transfer model based on flow patterns

In this Section, the heat and mass transfer of high-concentration NH_3/H_2O is investigated by combining equilibrium and non-equilibrium models. The vapor and liquid of NH_3/H_2O are co-current and flow vertically downward. The heat transfer model of pure NH_3 is taken as a starting point. The equilibrium model is developed in the

Table 1
Numerical and experimental research of NH_3/H_2O absorption in PHEs and other channels.

Study	Research method	Equilibrium conditions	Liquid phase[a]				Vapor phase[a]				Flow configuration
			Heat transfer	Mass transfer	*MC*	Flow	Heat transfer	Mass transfer	*MC*	Flow	
					PHEs						
Kang et al. [21]	Model	Interface equilibrium	α_{i_L} − EC α_L − EC	F_L − EC	0.272–0.438	Downward	α_{V_i} − EC	F_V − EC	0.965–0.983	Upward	Bubble mode Coolant upward
Kang et al. [22]	Model	Interface equilibrium	α_{i_L} − EC α_L − EC	F_L − HMTA	0.268–0.442	Downward	α_{V_i} − EC	F_V − HMTA	>0.987	Upward	Falling film mode Coolant upward
Lee et al. [24]	Experiment	–	α_L − EC	F_L[b] − EC	0–0.3	Downward	–	–	1	Upward	Bubble and falling film modes Coolant upward
Cerezo et al. [5]	Experiment	Liquid equilibrium	α_L − measured	F_L − measured	0.29–0.334	Upward	–	–	1	Upward	Bubble mode Coolant downward
Cerezo et al. [6]	Model Experimental validation	Interface equilibrium	α_{i_L} − EC α_L − EC	F_L − EC	0.29–0.339	Upward	α_{V_i} − EC	F_V − EC	1	Upward	Bubble mode Coolant downward
Jung et al. [20]	Experiment	–	α_L − EC	–	0.49–0.55	Upward	–	–	1	Upward	Bubble mode Coolant downward
Triché et al. [44]	Model Experimental validation	Interface equilibrium	α_{i_L} − HMTA α_L − EC	F_L − EC	0.433–0.500	Downward	α_{V_i} − EC	F_V − HMTA	0.991–0.999	Downward	Falling film mode Coolant upward
					Other channels						
van de Bor et al. [45]	Experiment	–	α_L	–	0.09–0.25[c]	Downward	–	–	0.44–0.83[c]	Downward	NH_3/H_2O in annulus Coolant upward
Fronk and Garimella [16,17]	Experiment& Model	Interface equilibrium	α_L − EC	–	0.4–0.96[c]	Horizontal	α_{V_i} − EC	F_V − HMTA	0.8–0.99[c]	Horizontal	NH_3/H_2O in tubes Coolant counter current
Chandrasekaran et al. [7]	Experiment& Model	Interface equilibrium	α_L − EC	–	0.375–0.522	Downward	α_{V_i} − EC	F_V − HMTA	>0.975	Upward& downward	NH_3/H_2O in shell side Coolant upward
Aminyavari et al [2,3]	Model Experimental validation	Interface equilibrium	α_{i_L} − HMTA	F_L − EC	0.232–0.484	Downward	α_{V_i} − EC	F_V − HMTA	0.992–0.999	Upward& downward	Falling film mode Coolant upward

[a] EC: empirical correlation; HMTA: heat and mass transfer analogy.
[b] This MTC is defined differently than by the other researchers.
[c] These mass concentrations are determined by the bulk mass concentration and vapor quality.

approximately-linear temperature glide region, where the interface temperature is equal to the local equilibrium temperature. The equilibrium temperature is a function of the overall bulk concentration and vapor quality. In the non-linear temperature glide region, the interface temperature deviates from the equilibrium temperature of the overall bulk concentration, and the non-equilibrium model applies. The non-equilibrium model applies at the beginning of the condensation, and transforms into the equilibrium model as the condensation proceeds.

2.1. Pure NH_3 condensation model

In a previous paper, the authors have developed a flow pattern-based model of pure NH_3 for PHEs [42]. As shown in Eq. (5), it is divided into convective condensation and combined condensation according to the liquid Weber number, We_L. The non-dimensional numbers are given in Eqs. (6)-(8). The liquid only HTCs are calculated according to the single-phase correlations in Supplementary material A. Convective condensation applies to full film flow, where the wall surface is completely wetted by the liquid. The vapor has a larger velocity than the liquid, and the interfacial shear force promotes the convection. All the heat is transferred through the liquid film. Combined condensation is applicable to partial film flow, which includes convective condensation and gravity-controlled condensation. Convective condensation happens in the wetted areas, while gravity-controlled condensation dominates in the dry zones [42].

Table 2
Range of experimental data [43].

NH_3 *MCs*	G	x	P
–	$kgm^{-2}s^{-1}$	–	kPa
80 %-96 %	32–86	0.08–0.65	610—780

the equilibrium temperature is shown as a function of overall bulk mass concentrations and vapor qualities. The relation of the vapor and liquid mass concentrations is explained accordingly. The heat transfer deterioration is contributed by the concentration gradient, which is quantified using the temperature gradient[19,48]. The thermodynamic properties of NH_3/H_2O are calculated using Refprop 10.0[25], while the transport properties of the mixture use Conde [11].

The flow patterns of high-concentration NH_3/H_2O are full film flow and partial film flow in the tested range [43]. Since high-concentration NH_3/H_2O has similar transport properties as pure NH_3, the transition criterion of NH_3 is considered as the starting point. It is full film flow when $We_L \geqslant 0.12$, and changes to partial film flow when $We_L < 0.12$. We_L is the ratio of liquid inertia to surface tension, which indicates the liquid film distribution and wetting characteristics. The condensation mechanism is distinguished accordingly. [42].

The mechanism is convective condensation for full film flow. The mixture condensation HTCs are predicted by modifying the SBG method in Eq. (9) and using the overall bulk concentration. The first term is the ideal heat transfer resistance of the NH_3/H_2O mixture. It is calculated by referring to Eq. (5) and using the mixture fluid properties at an equilibrium state. The second term accounts for the additional heat transfer resistance because of mass transfer. The additional resistance is proportional to the gradient of temperature glide indicated by dT/dh, which is calculated for the constant bulk concentration, operating pressure and local vapor quality. It quantifies the contribution of sensible heat. The additional resistance approaches 0 when the fluid becomes liquid only, where the phase change is finished. According to the experimental data, the apparent HTCs show noticeable sensitivity to mass fluxes [43]. The vapor is in contact with the two-phase interface to enable the phase change. The vapor is transferred from the bulk and towards the interface, where the vapor layer with a concentration gradient is penetrated by diffusion and convection. The concentration gradient shows the stratification effect. Larger mass fluxes promote the convection and reduce the concentration gradient [50]. The additional resistance is intensified by the stratification effect, but is alleviated by the momentum effect. The dominance of these effects is quantified using the liquid Froude number, Fr_L, which is the ratio of inertia to gravity as shown in Eq. (8). Large mass fluxes promote the mixing and mass transfer. As shown in Fig. 4, lower NH_3 concentration increases the additional resistance since the concentration gradient is aggravated. The influence of bulk concentration is also involved. The parameters 2.25 and 0.7 are the results of multi-variable regression analysis. Since it is convective condensation, the momentum effect is dominant.

$$\begin{cases} \alpha_{cc} = \alpha_{LO}\left(0.17Co^{-1.12}Fr_L^{-0.2} + (1-x)^{0.748}\right) & We_L \geqslant 0.12, \quad \text{convective condensation} \\ \alpha_c = \dfrac{We_L}{0.12}\alpha_{cc} + \left(1 - \dfrac{We_L}{0.12}\right)\alpha_{gc} & We_L < 0.12, \quad \text{combined condensation} \\ \alpha_{gc} = 0.36Co^{-0.28}\left(\dfrac{g\rho_L(\rho_L-\rho_V)\Delta h_{LV}\lambda_L^3}{\mu_L \Delta T d_h}\right)^{0.25} Pr_L^{0.333} \end{cases} \tag{5}$$

$$We_L = \frac{\rho_L v_L^2 d_h}{\sigma} = \frac{G^2(1-x)^2 d_h}{\rho_L \sigma} \tag{6}$$

$$Co = \left(\frac{\rho_V}{\rho_L}\right)^{0.5}\left(\frac{1-x}{x}\right)^{0.8} \tag{7}$$

$$Fr_L = \frac{G^2}{\rho_L^2 g d_h} \tag{8}$$

2.2. Equilibrium model in approximately-linear temperature glide region

The authors have measured the condensation of high-concentration NH_3/H_2O within PHEs including apparent HTCs and frictional pressure drop. The details of the experimental setup and methodology are provided in Tao et al. [43]. Table 2 gives the range of experimental data. The representative data are presented in Fig. 4, as well as the HTCs of pure NH_3 [41]. The averaged uncertainty of all the apparent HTCs is ± 12.9 %. Lower mass concentrations reduce the apparent HTCs. All the measured data are in the approximately-linear temperature glide region referring to Fig. 1. The vapor is in equilibrium with the liquid, and an equilibrium model is developed. In Fig. B1 of Supplementary material B,

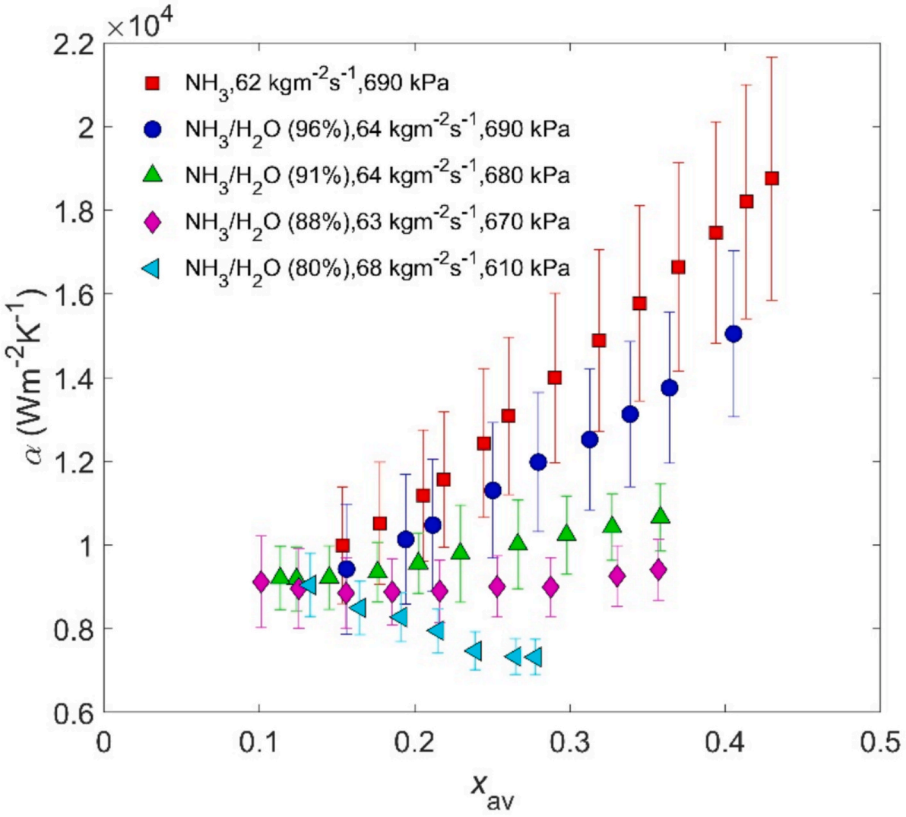

Fig. 4. Apparent HTCs for NH_3/H_2O of different mass concentrations and HTCs for pure NH_3 [41,43].

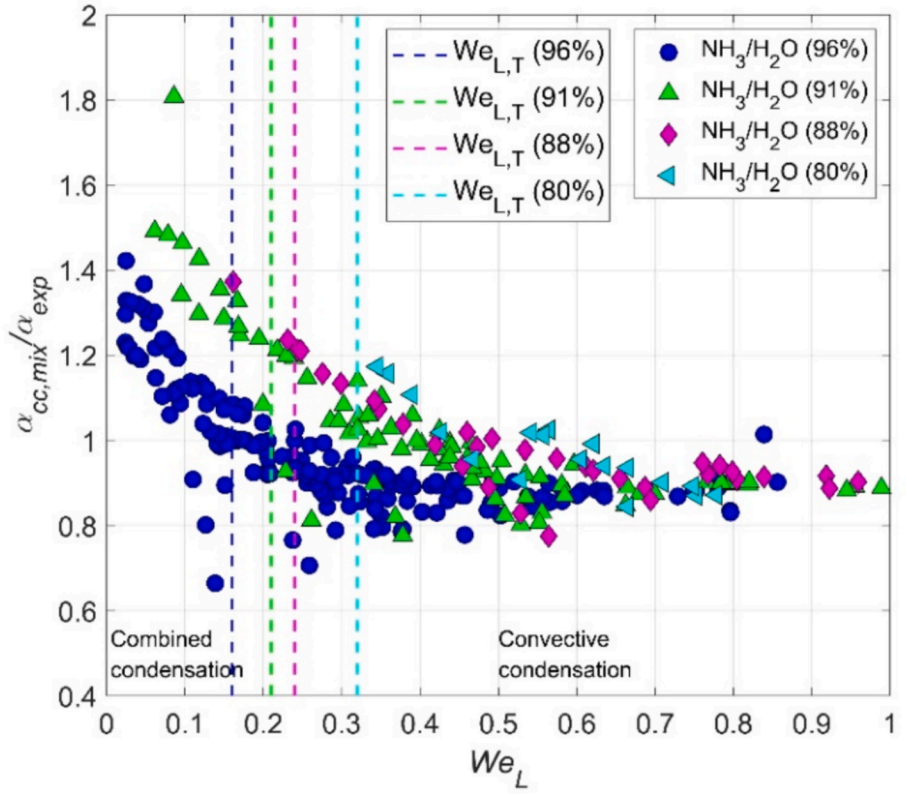

Fig. 5. Applicability of the correlation of convective condensation (Eq. (9)) in terms of We_L.

$$\alpha_{cc,mix} = \left(\underbrace{\alpha_{cc,mix0}^{-1}}_{\text{ideal heat transfer resistance of } NH_3/H_2O} + \underbrace{xc_{p,V}\frac{dT}{dh}\left(2.25MCFr_L^{0.7}\alpha_V\right)^{-1}}_{\text{additional resistance because of mass transfer}} \right)^{-1} \quad (9)$$

$We_L \geqslant We_{L,T}$, convective condensation

To validate the transition criterion of the condensation mechanism, the predicted values according to Eq. (9) are compared with all the experimental data in Fig. 5. The agreement is reasonable for large We_L. The experimental data are mostly over-predicted for small We_L, where partial film flow prevails. The transition value is 0.12 for pure NH_3 [42]. In terms of the mixtures, the transition value becomes larger for lower NH_3 concentration. As discussed in Tao et al. [43], lower concentrations increase the surface tension, which hinders the wetting of the surface and promotes partial film flow. In Eq. (10), the transition criterion is proposed as a function of the overall mass concentration. The transition lines are presented in Fig. 5, where the heat transfer deviates from convective condensation on the left of the transition lines.

$$We_{L,T} = 1.12 - MC \quad (10)$$

Partial film flow is composed of wetted areas and dry zones. The heat transfer is a combination of convective condensation and gravity-controlled condensation. The mixture correlation of combined condensation is given in Eq. (11). The heat transfer at the wetted area is the same as full film flow and is predicted using Eq. (9). In the dry zones, the additional resistance is also calculated with the SBG method as shown in Eq. (12). The determination of the mass concentration and dT/dh is the same as for Eq. (9). The stratification effect is strong for gravity-controlled condensation. The vapor has a large resistance to penetrate the layer of concentration gradients. The resulting heat transfer deterioration is quantified by a factor based on Fr_L and MC. The parameters are derived from the experimental data. The factor is smaller than 1 and increases with large mass fluxes.

$$\alpha_{c,mix} = \frac{We_L}{We_{L,T}}\alpha_{cc,mix} + \left(1 - \frac{We_L}{We_{L,T}}\right)\alpha_{gc,mix} \quad (11)$$

$We_L < We_{L,T}$, combined condensation

$$\alpha_{gc,mix} = \left(\underbrace{\alpha_{gc,mix0}^{-1}}_{\text{ideal heat transfer resistance of } NH_3/H_2O} + \underbrace{xc_{p,V}\frac{dT}{dh}\alpha_V^{-1}}_{\text{additional resistance because of mass transfer}} \right)^{-1} \underbrace{e^{-0.4MCFr_L^{-0.4}}}_{\text{stratifying effect}} \quad (12)$$

Fig. 6 presents the prediction of the proposed equilibrium model validated by the experimental apparent HTCs [43]. The agreement is good with 96.6 % of the experimental data predicted within ± 30 %. Combined condensation shows the smallest values because of the stratification effect.

Eqs. (9)-(12) are derived under the framework of the equilibrium

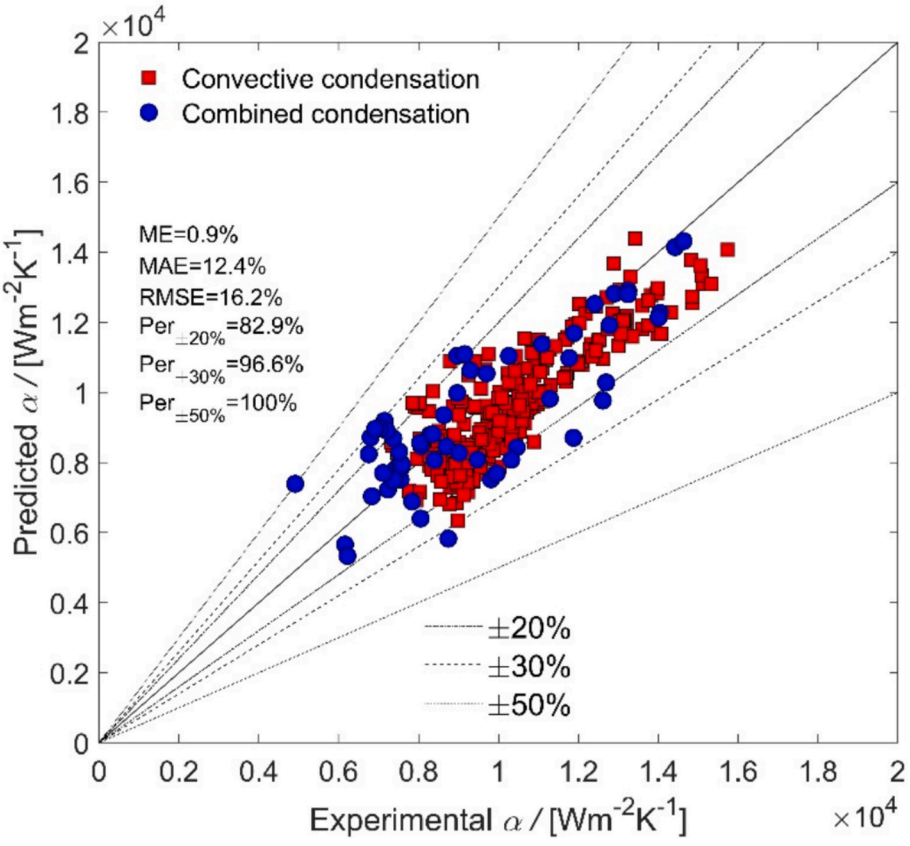

Fig. 6. Comparison of NH_3/H_2O condensation HTCs with the proposed equilibrium model. Mean error (ME): $\frac{1}{n}\sum_1^n \frac{\alpha_{pre}-\alpha_{exp}}{\alpha_{exp}}$; Mean absolute error (MAE): $\frac{1}{n}\sum_1^n \frac{|\alpha_{pre}-\alpha_{exp}|}{\alpha_{exp}}$; Root mean squared error (RMSE): $\sqrt{\frac{1}{n}\sum_1^n \left(\frac{\alpha_{pre}-\alpha_{exp}}{\alpha_{exp}}\right)^2}$; $Per_{\pm 20\%}$: Percentage of experimental data within ±20%; $Per_{\pm 30\%}$: Percentage of experimental data within ±30%; $Per_{\pm 50\%}$: Percentage of experimental data within ±50%.

model, and the interface concentration is identical to the overall bulk concentration, where the vapor bulk is in equilibrium with the liquid bulk. These equations can be adjusted to the non-equilibrium model where the interface concentration deviates from the equilibrium conditions. The interface concentration is used to calculate the additional resistance and is determined by solving the mass transfer equations.

2.3. Non-equilibrium model in non-linear temperature glide region

In the non-linear temperature glide region of Fig. 1, the heat transfer is coupled with the mass transfer. The interface temperature deviates from the bulk equilibrium temperature, and the apparent HTCs are under-predicted[17]. An improved non-equilibrium model is proposed starting from the equilibrium model discussed in Section 2.2. The actual interface temperature and mass concentration are determined using the film theory. The following assumptions are adopted to solve the energy and mass balances:

- The vapor interface is in equilibrium with the liquid interface, both of which are in saturated condition.
- The liquid mass transfer resistance is neglected. The liquid bulk concentration is equal to the liquid interface concentration.
- The condensation heat transfer is driven by the temperature difference between the interface and the wall. The condensation HTCs are calculated with the equilibrium model.
- The vapor mass transfer follows the film theory. It is represented by the vapor bulk concentration and vapor interface concentration.
- The sensible heat transfer between the vapor and interface is single-phase heat transfer. The heat transfer area is the same as the wall surface.
- The frictional pressure drop is negligible for heat and mass transfer calculations.

During the visualization of condensation within PHEs, the liquid phase is observed to be turbulent and well mixed in the corrugated channels[41]. The strong convection significantly reduces the liquid mass transfer resistance. The dominance of mass transfer resistance is widely discussed[19,23,36]. The mass transfer resistance of liquid is minor compared with that of vapor[17,48,50]. Consequently, it is reasonable to neglect the liquid mass transfer resistance.

Since the equilibrium model is flow pattern-based, the heat transfer prediction reveals actual flow characteristics. The vapor quality decreases during condensation. The corresponding reduction of flow velocities transforms the flow patterns, which determines the local HTCs. The frictional pressure drop affects heat and mass transfer by reducing the saturated pressure in the flow direction. The effect on fluid properties is small and is neglected, as will be discussed separately in Section 3.3. The model applies to the condition that liquid and vapor flow co-currently downward.

2.3.1. Vapor heat and mass transfer

The single-phase heat transfer of vapor is calculated with Eq. (13). α_V is the vapor HTC and is calculated using the correlations of the VDI, which are given in Supplementary material A[30]. The heat transfer area, A, is the effective area of the corrugated surface. The interface is parallel to the wall surface so that the influence of interfacial roughness is accounted for. The log mean temperature difference between the vapor and interface is determined. The vapor is cooled when it has a higher temperature than the interface. The vapor is heated when it has a lower temperature than the interface under the condition that the vapor concentration is equal to or higher than the interface.

$$\dot{Q}_V = \alpha_V A \frac{\left(T_{V,out} - T_{i,out}\right) - \left(T_{V,in} - T_{i,in}\right)}{\ln \frac{T_{V,out} - T_{i,out}}{T_{V,in} - T_{i,in}}} = \dot{m}_V c_{p,V}\left(T_{V,in} - T_{V,out}\right) \tag{13}$$

In Eq. (14), the mass transfer from the vapor to the interface is calculated according to the film theory [37]. It is the same as the vapor mass transfer calculated using Eq. (2). The liquid MTC is so large that the liquid bulk concentration is equal to the liquid interface concentration. The term liquid mass transfer is simplified. β_V is the vapor MTC. In Eqs. (15)-(16), it is determined using the heat and mass transfer analogy with vapor Sherwood number, Sh_V [8]. C_V is the vapor density in the mole base and is illustrated in Eq. (17).

$$N_{NH_3} + N_{H_2O} = F_V \ln\left(\frac{z - x_{Vi}}{z - x_V}\right) = \beta_V C_V \ln\left(\frac{z - x_{Vi}}{z - x_V}\right) \tag{14}$$

$$\beta_V = \frac{Sh_V D_V}{d_h} \tag{15}$$

$$Sh_V = Nu_V \left(\frac{Sc_V}{Pr_V}\right)^{1/3} \tag{16}$$

$$C_V = \frac{\rho_V}{x_V M_{NH_3} + (1 - x_V) M_{H_2O}} \tag{17}$$

2.3.2. Total and liquid heat transfer

The total transferred heat includes the sensible heat of vapor and liquid, as well as the latent heat. As shown in Eq. (18), the total heat transfer is driven by the temperature difference between the interface and cooling water. α_{mix} is the mixture HTC and is calculated according to Eqs. (9)-(12). The temperature glide of the mixture is quantified at the interface, and the condensation HTC is consistent. The difference with the equilibrium model is the concentration. It is the actual interface concentration instead of the equilibrium concentration. The total heat in the NH_3/H_2O side is determined by the energy balance of the vapor and liquid phases. The total heat is taken away by the cooling water.

$$\begin{aligned} \dot{Q}_T &= \frac{A}{\frac{1}{\alpha_{mix}} + \frac{d_p}{\lambda_{wall}} + \frac{1}{\alpha_w}} \frac{\left(T_{i,in} - T_{w,out}\right) - \left(T_{i,out} - T_{w,in}\right)}{\ln \frac{T_{i,in} - T_{w,out}}{T_{i,out} - T_{w,in}}} \\ &= \dot{m}_{aw}\left(h_{aw,in} - h_{aw,out}\right) \\ &= \dot{m}_{V,in} h_{V,in} + \dot{m}_{L,in} h_{L,in} - \dot{m}_{V,out} h_{V,out} - \dot{m}_{L,out} h_{L,out} \\ &= \dot{m}_w c_{p,w}\left(T_{w,out} - T_{w,in}\right) \end{aligned} \tag{18}$$

The liquid is subcooled. The liquid temperature is derived using an analytical framework of conservation law and is solved numerically involving the variable fluid properties[31]. It is calculated using Eq. (19). This analysis is based on the film condensation of mixtures and considers vapor superheating[31]. It is demonstrated that the inertia and convection are negligible for liquid heat transfer[31]. It is inferred that Eq. (19) is accurate for fully developed flow.

$$T_{L,out} = T_{wall,out} + 0.31\left(T_{i,out} - T_{wall,out}\right) \tag{19}$$

2.3.3. Mass balance and species balance

The two-phase flow of NH_3/H_2O follows the conservation of mass and mixture components. In Eq. (20), the overall mass flow of vapor and liquid at the inlet is equal to that at the outlet. The conservation also applies to the NH_3 component as illustrated in Eq. (21). The simultaneous conservation of H_2O is derived from Eqs. (20)-(21). The overall and NH_3 condensing fluxes are calculated with Eqs. (22)-(23), which are in the mass base. To close Eq. (14), the units of condensing fluxes need to be unified.

$$\dot{m}_{V,in} + \dot{m}_{L,in} = \dot{m}_{V,out} + \dot{m}_{L,out} \tag{20}$$

$$\dot{m}_{V,in} MC_{V,in} + \dot{m}_{L,in} MC_{L,in} = \dot{m}_{V,out} MC_{V,out} + \dot{m}_{L,out} MC_{L,out} \tag{21}$$

$$\dot{m}'' = \frac{\dot{m}_{V,in} - \dot{m}_{V,out}}{A} \tag{22}$$

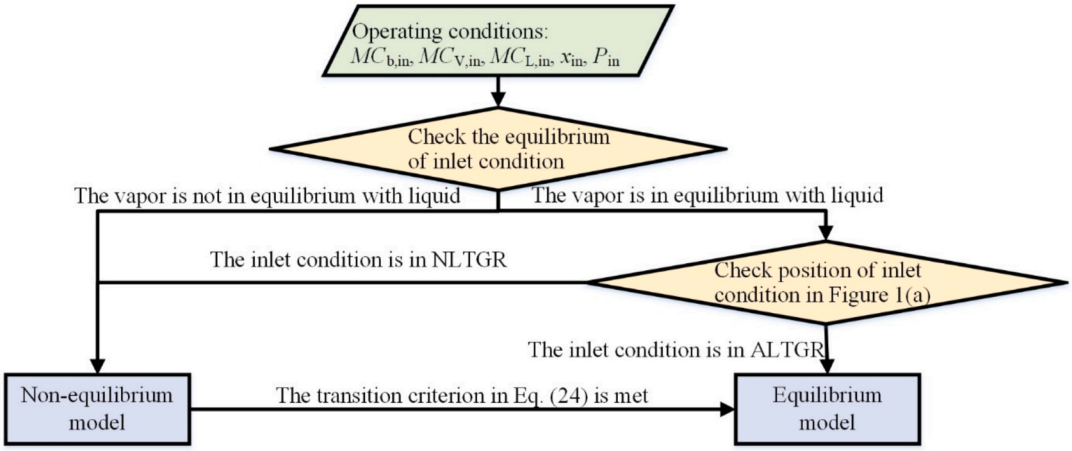

Fig. 7. The flow diagram used to distinguish between non-equilibrium and equilibrium models. ALTGR: Approximately-linear temperature glide region; NLTGR: Non-linear temperature glide region.

$$\dot{m}''_{NH_3} = \frac{\dot{m}_{V,in} MC_{V,in} - \dot{m}_{V,out} MC_{V,out}}{A} \tag{23}$$

2.4. Implementation of the method

The proposed model is implemented numerically using a control volume approach. Eqs. (13)-(23) are solved for each control volume where the fluid properties and HTCs are almost constant, and thus the logarithmic mean temperature difference applies to each control volume. The heat and mass transfer are coupled through the local temperature and concentration difference by calculating the interfacial condition. The equilibrium and non-equilibrium models are combined for prediction. The thermodynamic states of NH_3/H_2O and cooling water at the inlet are the boundary conditions.

Fig. 7 shows how to distinguish between non-equilibrium and equilibrium models. $MC_{b,in}$, $MC_{V,in}$ and $MC_{L,in}$ are the overall concentration, vapor bulk concentration and liquid bulk concentration at the inlet. For given inlet conditions, if the vapor is not in equilibrium with liquid, non-equilibrium model is applicable. The case in Section 2.5.1 falls into this category. Otherwise, if the vapor is in equilibrium with liquid, the condition needs to be located according to the profile of the temperature glide for the corresponding pressure, which is similar to Fig. 1(a). Non-equilibrium model applies for data in non-linear temperature glide region, which is the case in Section 2.5.2. The data in approximately-linear temperature glide region is calculated using the equilibrium model. As the condensation proceeds, the state moves into approximately-linear temperature glide region. Once Eq. (24) is met and the interface concentration is close to the overall bulk concentration, it is changed into equilibrium model.

$$|MC_i - MC_b| \leqslant 0.001 \tag{24}$$

The solution of the heat and mass transfer includes energy conservation, mass conservation and mixture components conservation. Fig. 8 is the flow diagram of the solver. The inlet conditions of NH_3/H_2O and cooling water are the boundary conditions. The model is implemented as follows:

1. The model is initialized by discretizing the control volumes. The distribution of T, x and MC is assumed.
2. Fluid properties are calculated for all the control volumes according to the local conditions.
3. The heat and mass transfer coefficients are predicted. The condensation HTCs of NH_3/H_2O are calculated according to Eqs. (9)-(12) with interface concentration. The vapor HTCs are calculated using the single-phase correlations in Eqs. (A1)-(A5). The vapor MTCs are determined by heat and mass transfer analogy as indicated in Eqs. (15)-(16). The HTCs of cooling water are predicted with Eqs. (A1)-(A5).
4. The governing equations are solved for each control volume. For the non-equilibrium model, Eqs. (13)-(14), (18)-(23) are solved simultaneously in discretized forms. The equilibrium model is slightly different. Since the vapor bulk is in equilibrium with the liquid bulk, the equations are closed without Eq. (14). Referring to Eq. (14), the condensing flux becomes zero as the vapor concentration gradient diminishes, which does not reflect the actual condensing flux determined by the temperature gradient. The non-equilibrium model is transformed into the equilibrium model.
5. The residuals between two successive iterations are estimated. Four residual values are calculated for the non-equilibrium model. The equilibrium model has one less residual value since the vapor mass transfer equation is not needed. The iteration error is the norm of the maximum relative residuals. The iteration is finished when the error is smaller than the tolerance. Otherwise, the iteration variables are updated, and a new iteration is started.
6. To simplify the calculation, the frictional pressure drop is neglected for the iteration. When the iteration is finished, the frictional pressure drop of NH_3/H_2O is estimated separately with Eq. (26). The pressure drops of liquid phase, vapor phase and cooling water are calculated with Darcy friction factor in Eqs. (A1)-(A4).

2.5. Analysis of heat and mass transfer model

The model is discussed for two sets of operating conditions. The two-phase NH_3/H_2O flows vertically downward for both cases.

2.5.1. NH_3/H_2O with mass concentration of 59 %

The experimental data of Triché et al. [44] are used for the validation and analysis of the model. The geometrical parameters of the tested PHE are given in Table 3 as Type 1 [39]. Sixteen plates form fifteen channels including seven NH_3/H_2O channels and eight cooling water channels. The working fluids are assumed to distribute uniformly among the channels.

Table 4 presents the inlet conditions. NH_3/H_2O is two-phase. The vapor and liquid are not in equilibrium and are mixed at the inlet. The liquid has a higher temperature than the vapor at the inlet. The bulk vapor quality is 0.24, while the overall bulk mass concentration is 59 %. The cooling water flows counter-currently to NH_3/H_2O. The heat exchanger is divided into 800 control volumes so that the results are independent of the control volume number.

Fig. 9(a) presents the temperature distributions including the

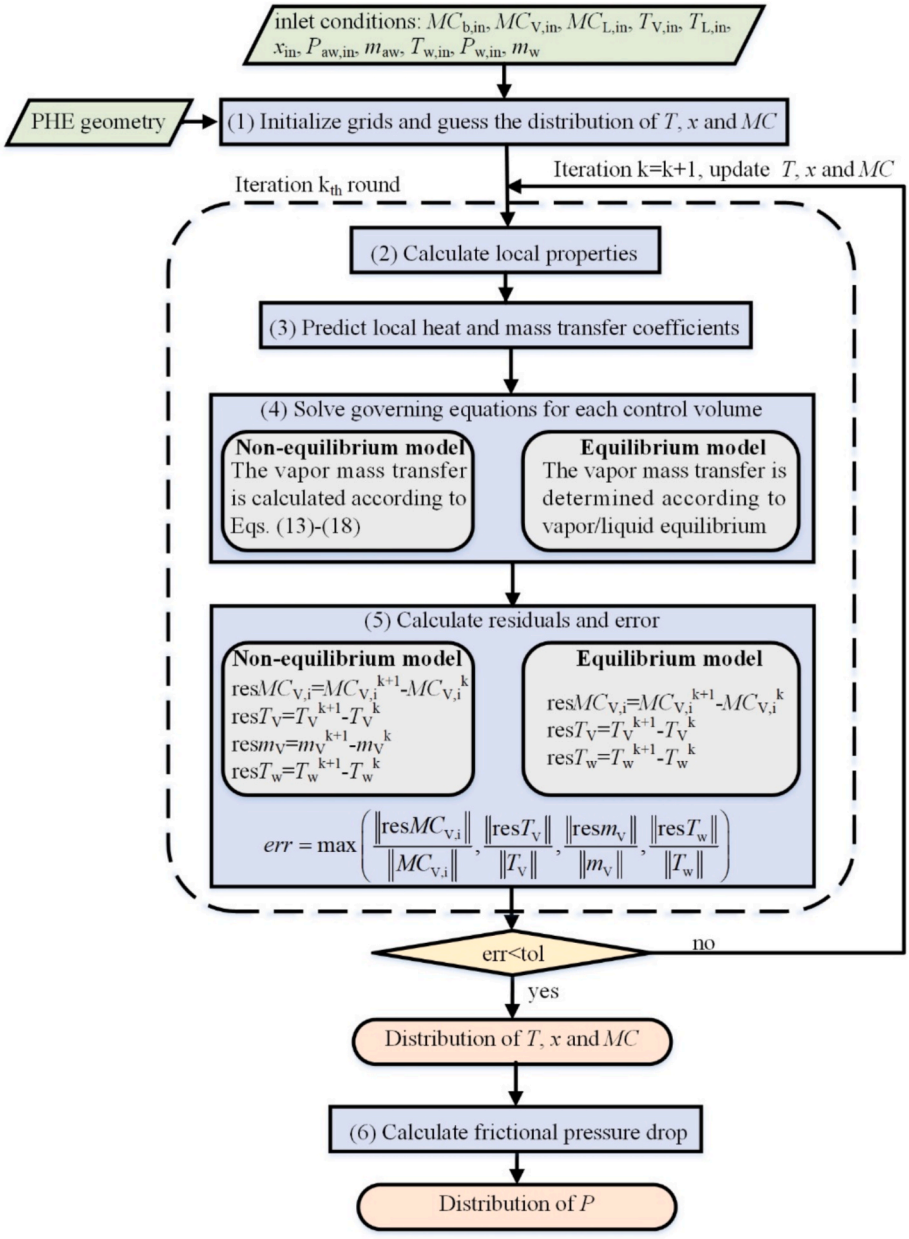

Fig. 8. Solver for heat and mass transfer calculation combining equilibrium and non-equilibrium models.

Table 3
Geometrical parameters of the PHEs.

Type	Plate number	L_p	W_p	A	d_h	β	ϕ	d_g	d_p	Λ_{wave}
–	–	mm	mm	m^2	mm	–	–	mm	mm	mm
1	16	668	95	0.896	2.99	63°	1.15	1.72	0.58	6.67
2	4	1283	95	0.246	2.99	63°	1.15	1.72	0.58	6.67

Table 4
Inlet conditions of the working fluids [44].

Parameters	Units	NH_3/H_2O	Cooling water
$T_{L,in}$	°C	39.1	27.0
$T_{V,in}$	°C	25.5	–
P_{in}	kPa	607	101
$\dot{m}$	kg/s	0.0211	0.33
MC_b	–	59 %	–

predicted and experimental values. The liquid temperature of NH_3/H_2O decreases from the inlet to the outlet. The vapor temperature increases close to the inlet as it is heated by the interface. It reaches the maximum temperature at 1/4 of the heat exchanger length, where the temperature is equal to the interface. And then, the vapor is cooled. The equilibrium temperature of the overall bulk and interface temperature are also given. In the inlet region, the interface temperature is higher than the equilibrium temperature. The cooling water temperature shows a good agreement with the experimental values, while the predicted wall temperature is not as sharp as the experiment.

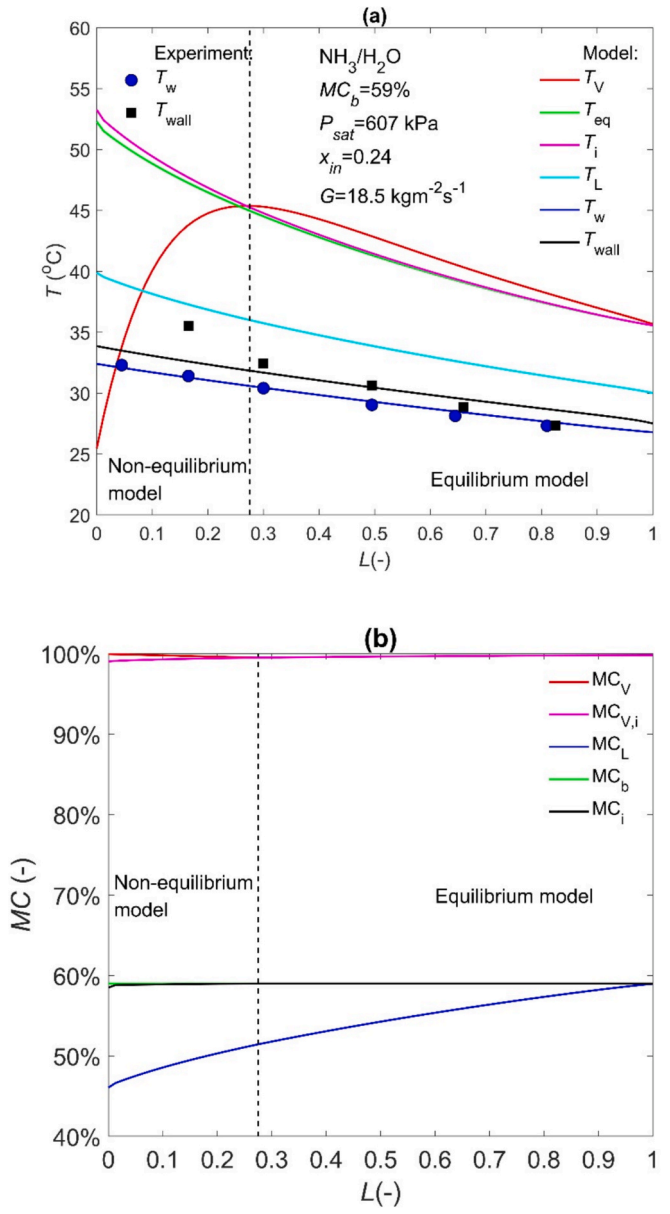

Fig. 9. (a) The predicted and experimental temperature distributions; (b) The predicted mass concentration distributions.

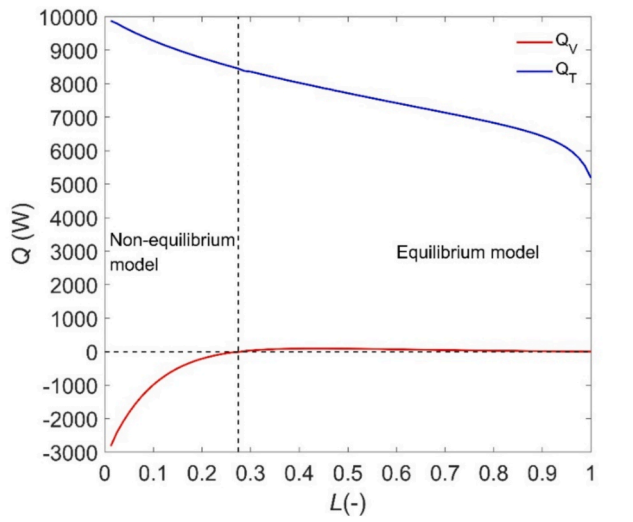

Fig. 10. The total and vapor heat flux distributions along the PHE.

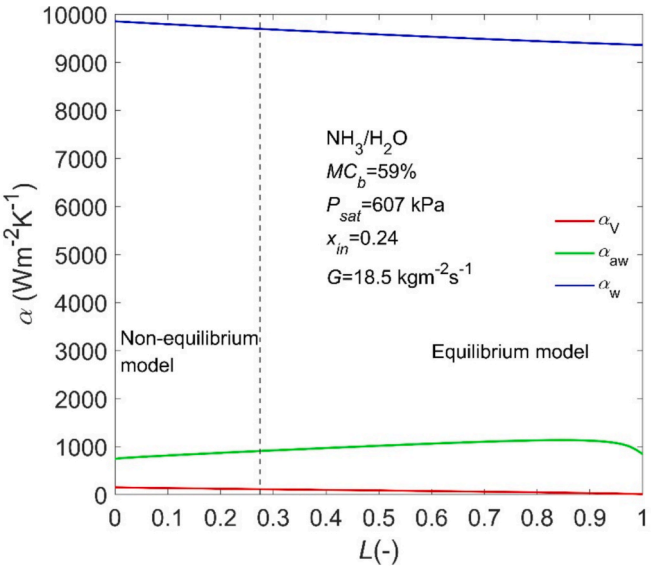

Fig. 11. The HTC distributions along the PHE including the vapor single-phase heat transfer, NH_3/H_2O condensation heat transfer and cooling water heat transfer.

In the inlet region of Fig. 9(b), the vapor bulk mass concentration is slightly higher than the vapor interface, and the difference diminishes in the flow direction. NH_3 is condensed, while H_2O flows from liquid to vapor. This condition corresponds to the interpretation of Figs. 3(a) and 3(c). In this region, the non-equilibrium model is applied. The non-equilibrium between the vapor and liquid results from the inlet condition. In the following region, the interface mass concentration is equal to the overall bulk mass concentration, and the equilibrium model applies. The liquid bulk mass concentration increases in the flow direction and approaches the overall bulk mass concentration of 0.59 at the outlet, where the condensation is finished.

Fig. 10 gives the heat flux profile. The heat exchanger length is non-dimensional (flow length/L_p). The actual heat transfer rate is the integral of the heat flux. The total heat flux decreases from the inlet to the outlet as the temperature driving force is reduced. The vapor is heated close to the inlet, and the heat flux is then negative. The latent heat released at the interface is transferred to the vapor and liquid. The vapor heat flux becomes positive when the vapor temperature is higher than the interface temperature. All the latent heat is transferred through the liquid to the wall. The predicted heat transfer rate is 7942 W and agrees reasonably well with the experimental value of 7549 W.

The variation of the HTCs is presented in Fig. 11. The condensation HTC of NH_3/H_2O is determined based on the interface concentration. This HTC increases slightly in the flow direction as the result of a decreasing temperature glide. It is combined condensation all over the PHE. This condensation correlation identifies the heat transfer deterioration because of the transition from full film flow to partial film flow. The influence of liquid film characteristics has been addressed by Triché et al. [44] and Chandrasekaran et al. [7]. The vapor HTC decreases because of the reduced vapor quality. The cooling water HTC is much larger.

More experimental data from Triché et al. [44] are compared with the model in Table 5. The heat transfer rates are accurately predicted with a relative error smaller than 6 %. The predicted values are slightly larger. The model assumes ideal flow distribution, which is difficult to realize in practice. During the experiments, the vapor phase had liquid entrainment at the inlet, which is not considered in the model. NH_3/H_2O is slightly subcooled at the outlet [44].

Table 5
Comparison of the predicted values with experimental results of Triché et al. [44].

States	$\dot{m}_{V,in}$	$\dot{m}_{L,in}$	$T_{V,in}$	$T_{L,in}$	$x_{V,in}$	$x_{L,in}$	P	$\dot{Q}_T$ Exp.	$\dot{Q}_T$ Pre.	Deviation
Unit	kg/s	kg/s	°C	°C	–	–	kPa	W	W	–
Case 1	0.0051	0.016	25.5	39.1	0.998	0.458	607	7549	7942	5.2 %
Case 2	0.0038	0.017	24.8	44.3	0.995	0.489	629	5871	6079	3.5 %
Case 3	0.0061	0.015	25.3	36.1	0.999	0.433	598	8872	9096	2.5 %
Case 4	0.0044	0.017	25.2	37.2	0.998	0.500	621	6400	6751	5.5 %
Case 5	0.0046	0.016	25.2	40.6	0.997	0.463	578	6975	7265	4.2 %
Case 6	0.0055	0.024	21.6	42.5	0.992	0.491	603	8437	8942	6.0 %
Case 7	0.0055	0.027	20.6	44.3	0.991	0.498	604	8723	9047	3.7 %
Case 8	0.0038	0.017	23.4	45.4	0.998	0.473	629	5991	6339	5.8 %
Case 9	0.0055	0.015	27.7	38.3	0.999	0.447	609	8069	8516	5.5 %
Case 10	0.0052	0.016	22.0	39.4	0.993	0.452	603	7536	7983	5.9 %

Table 6
Inlet conditions of the working fluids.

Parameters	Units	NH_3/H_2O	Cooling water
$T_{L,in}$	°C	70.6	8
$T_{V,in}$	°C	117.4	–
P_{in}	kPa	800	300
$\dot{m}$	kg/s	0.0049	0.05
Bulk MC	–	80 %	–

2.5.2. NH_3/H_2O with mass concentration of 80 %

The complete condensation is calculated to investigate the non-linear temperature glide and approximately-linear temperature glide. The inlet conditions are presented in Table 6. NH_3/H_2O has a bulk vapor quality of 0.99 and is close to saturated vapor. The vapor temperature is higher than the liquid temperature since the liquid is subcooled. The geometrical parameters of the PHE are given in Table 3 as Type 2. Four plates form three channels including one channel for NH_3/H_2O and two channels for cooling water. Two plates are effective for heat transfer. NH_3/H_2O flows counter-currently to the cooling water. According to the assessment of the impact of the control volume number, the heat exchanger is divided into 1000 control volumes.

Fig. 12(a) presents the temperature distributions. The NH_3/H_2O temperatures of vapor and liquid decrease from the inlet to the outlet. In the inlet region where the non-equilibrium model applies, the interface temperature is lower than the equilibrium temperature. The difference diminishes until zero, which indicates the beginning of the equilibrium model. The transition from non-equilibrium to equilibrium is gradual and is governed by the mass transfer of vapor. The vapor is saturated at the inlet where the temperature is the same as the equilibrium temperature. At the rest of the heat exchanger, the vapor temperature is higher than the local saturated temperature, and the vapor is superheated. The sensible heat of the vapor is removed through the interface. Once condensation happens at the inlet, the liquid has a large degree of subcooling. The subcooling degree decreases as more liquid is accumulated. The subcooling degree is 8 K at the outlet. The temperature difference between the interface and cooling water changes sharply in the non-linear temperature glide region, but is relatively constant in the approximately-linear temperature glide region. The pinch point temperature difference is reached approximately at 70 % of the heat exchanger length.

Fig. 12(b) shows the mass concentration profile. The vapor bulk mass concentration is equal to the overall bulk mass concentration (80 %) at the inlet, and increases in the flow direction. Both NH_3 and H_2O are condensed, which is indicated in Figs. 2(a) and 2(b). Because of mass transfer resistance, the vapor bulk mass concentration is lower than the vapor interface mass concentration, while the interface mass concentration is higher than the overall bulk mass concentration. The relation of the two-phase mass concentrations is explained in Fig. B2 of Supplementary material B. As the condensation proceeds, the vapor bulk and vapor interface become almost pure NH_3. The concentration

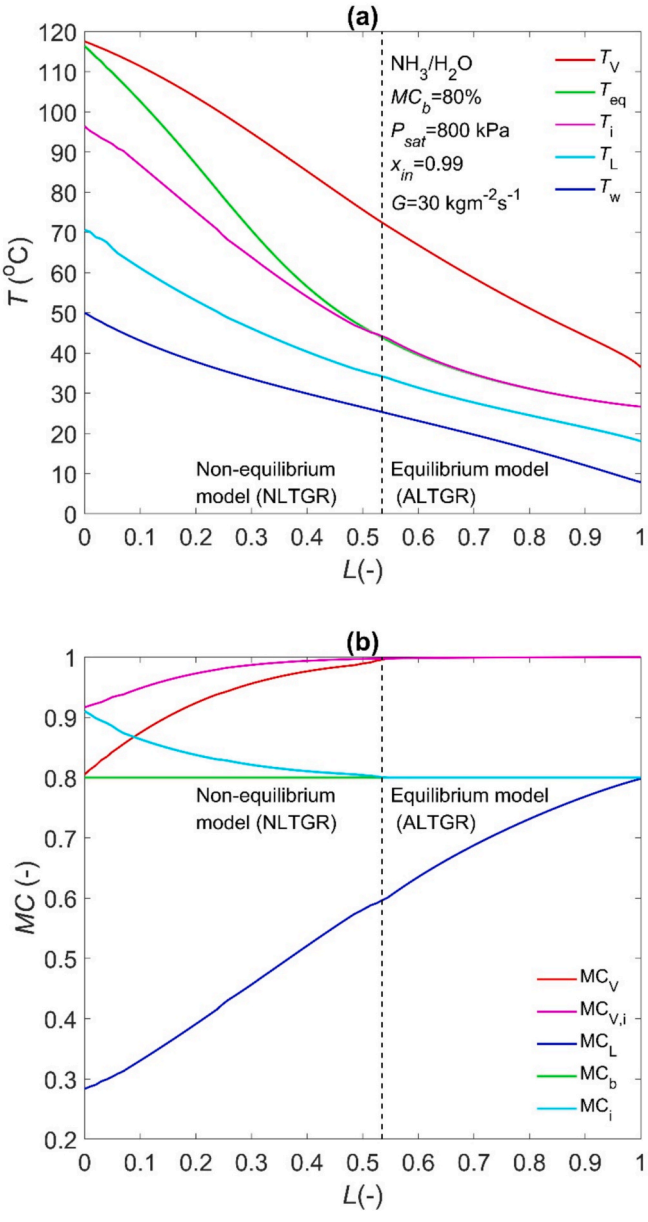

Fig. 12. (a) Temperature and (b) mass concentration distributions along the non-dimensional heat exchanger length for complete condensation. ALTGR: Approximately-linear temperature glide region; NLTGR: Non-linear temperature glide region.

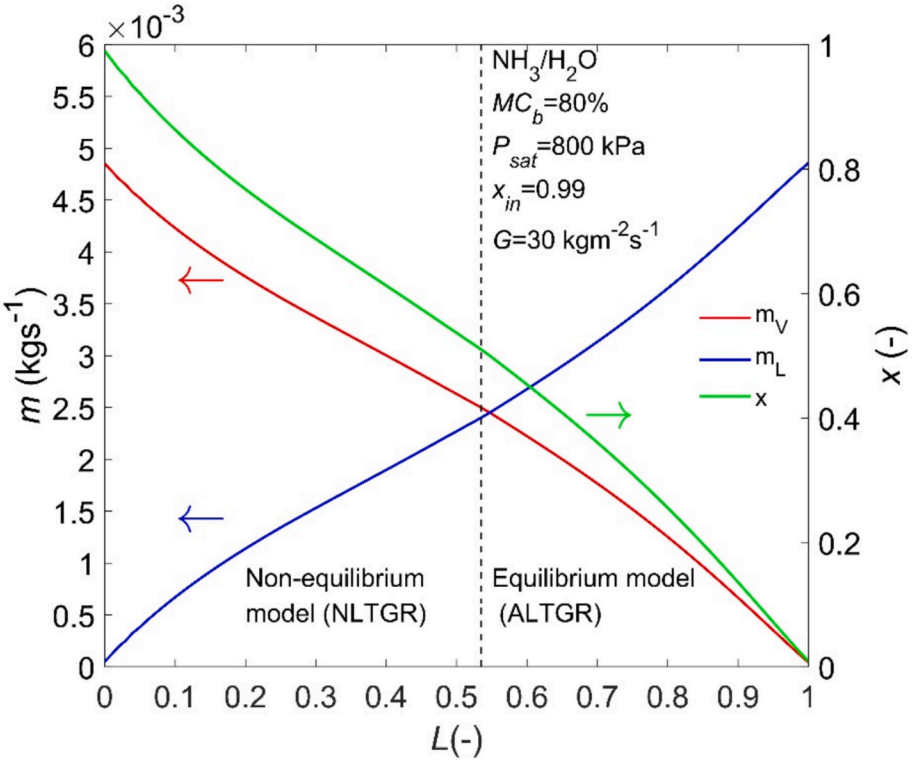

Fig. 13. The two-phase mass flow rates and vapor quality distributions along the PHE. ALTGR: Approximately-linear temperature glide region; NLTGR: Non-linear temperature glide region.

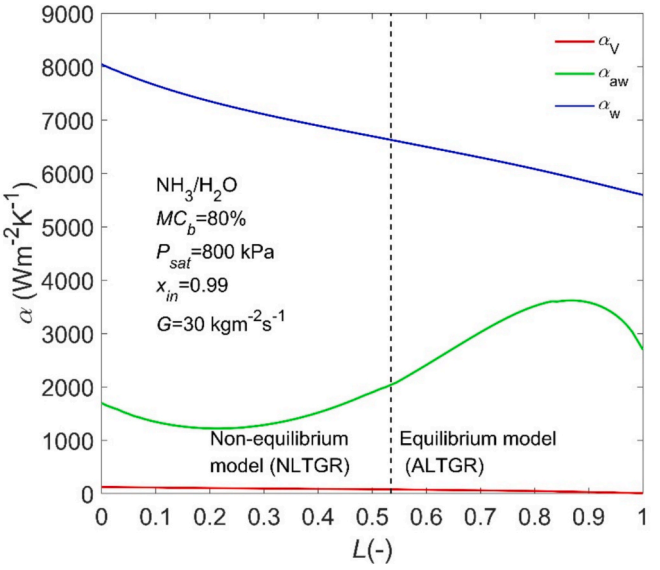

Fig. 14. The HTC distributions of complete condensation including the vapor single-phase heat transfer, NH_3/H_2O condensation heat transfer and cooling water heat transfer. ALTGR: Approximately-linear temperature glide region; NLTGR: Non-linear temperature glide region.

gradient diminishes. The interface mass concentration becomes equal to the overall bulk mass concentration. The liquid bulk mass concentration increases all the way until the overall bulk mass concentration is attained. The bulk system concentration is in equilibrium, and the equilibrium model applies.

The profiles of mass flow rates and vapor quality are given in Fig. 13. The vapor quality reaches 0.5 using 54 % of the heat transfer area. The vapor quality decreases smoothly all over the heat exchanger. The transfer of latent heat is stable. In the non-linear temperature glide region, the temperature driving force is large, and the sensible heat contributes noticeably to the total heat flux. Since the vapor mass flow rate is small close to the outlet, it is fully cooled through the interface as shown in Fig. 12(a).

Fig. 14 presents the HTC distributions during complete condensation. As the vapor quality decreases, the condensation HTC of NH_3/H_2O first increases and then decreases. The peak value is at the vapor quality of 0.2. The sensitivity of mixture HTC to vapor quality results from the conflicting effects of the convection and additional heat transfer resistance contributed by mass transfer. The mixture HTC is small in the non-linear temperature glide region where the temperature glide contributes significantly to the additional resistance. As indicated by Fig. 1(b), additional resistance is large for high vapor quality, which dominates over the strong convection. Additional resistance is alleviated for low vapor qualities. Combined condensation prevails all over the PHE. The cooling water HTC increases with higher temperature. The vapor HTC is very small.

In the above analysis, the prediction of both operating conditions starts with the non-equilibrium model close to the inlet, and ends up with the equilibrium model close to the outlet. Heat and mass transfer are solved for the non-equilibrium model. Superheated vapor condensation of the mixture is predicted by the equilibrium model. As the vapor concentration gradient becomes zero or the interface concentration approaches the bulk concentration, the non-equilibrium model is transformed into the equilibrium model. Eq. (24) is taken as the transition criterion, and the corresponding deviation between the interface temperature and bulk equilibrium temperature is smaller than 0.5 K. The influence on heat transfer is negligible, and the equilibrium model applies.

3. Frictional pressure drop model

The frictional pressure drops of pure NH_3 and high-concentration

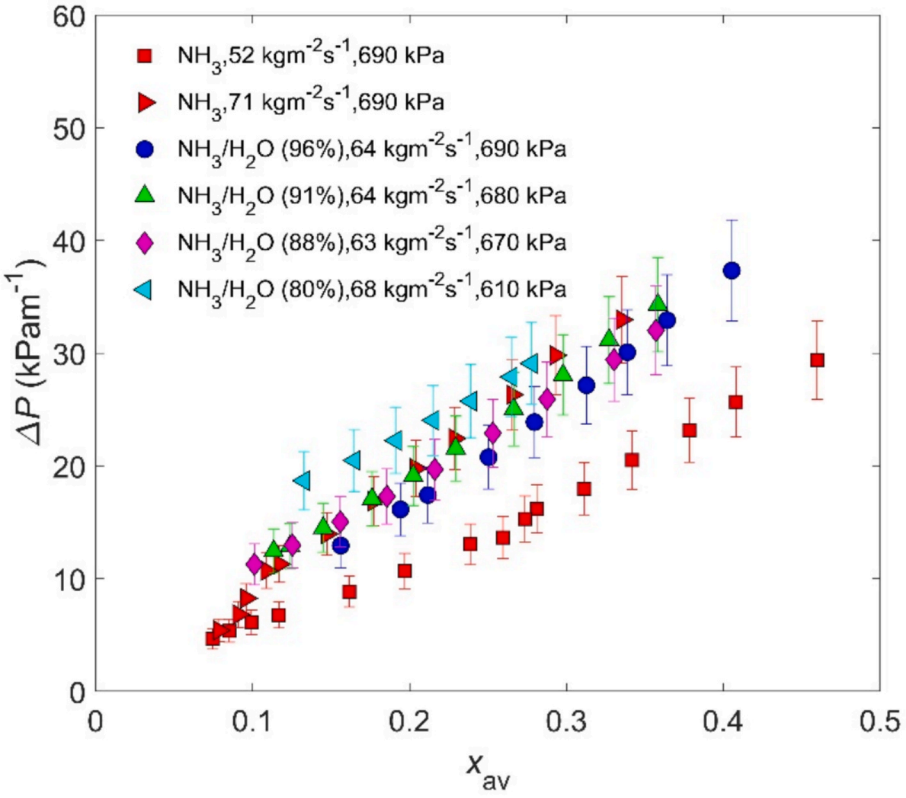

Fig. 15. Frictional pressure drop for pure NH_3 and high-concentration NH_3/H_2O [41,43].

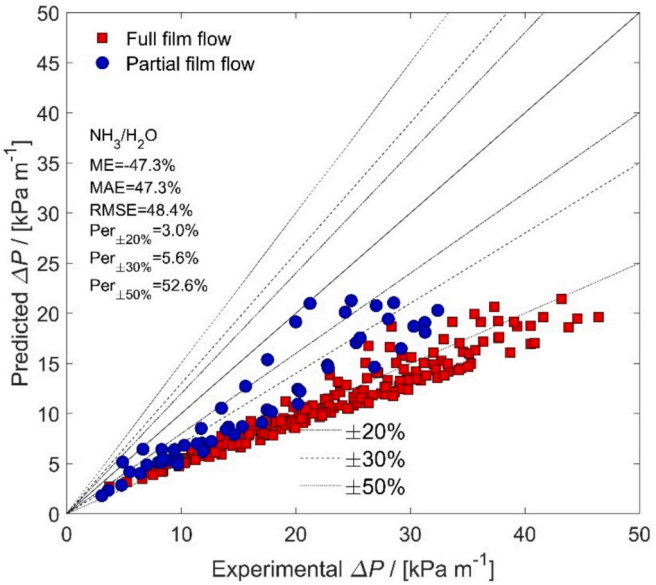

Fig. 16. Comparison of NH_3/H_2O frictional pressure drop with Eq. (25). Mean error (ME): $\frac{1}{n}\sum_1^n \frac{\Delta P_{pre}-\Delta P_{exp}}{\Delta P_{exp}}$; Mean absolute error (MAE): $\frac{1}{n}\sum_1^n \frac{|\Delta P_{pre}-\Delta P_{exp}|}{\Delta P_{exp}}$; Root mean squared error (RMSE): $\sqrt{\frac{1}{n}\sum_1^n \left(\frac{\Delta P_{pre}-\Delta P_{exp}}{\Delta P_{exp}}\right)^2}$; $Per_{\pm 20\%}$: Percentage of experimental data within ±20%; $Per_{\pm 30\%}$: Percentage of experimental data within ±30%; $Per_{\pm 50\%}$: Percentage of experimental data within ±50%.

NH_3/H_2O are compared in Fig. 15 [41,43]. The averaged uncertainty of all the frictional pressure drops is ± 14.1 %. The vapor and liquid of NH_3/H_2O flow co-currently and vertically downward. The pressure drops of inlet and outlet ports, the deceleration pressure rise, as well as elevation pressure rise are excluded from the measured pressure drop so that only the frictional pressure drop is discussed. Under similar mass fluxes and vapor qualities, the frictional pressure drops of NH_3/H_2O increase slightly with lower mass concentrations. NH_3 has a smaller frictional pressure drop than NH_3/H_2O.

3.1. Comparison with NH_3 frictional pressure drop model

A frictional pressure drop model has been developed for pure NH_3 based on separated flow, which is in the form of the Lockhart-Martinelli model and is shown in Eq. (25) [42]. Since mass transfer resistance has a negligible influence on frictional pressure drop, the model of pure NH_3 is expected to apply to high-concentration NH_3/H_2O. The comparison is presented in Fig. 16. The experimental data are under-predicted, but the trend is reasonable. Lockhart-Martinelli model interprets the primary characteristics of separated flow. The form is adopted for further analysis[9,28].

$$\Delta P_{TP} = \underbrace{\Delta P_L}_{\text{liqud pressure drop}} + \underbrace{2\sqrt{\Delta P_L \Delta P_V}}_{\text{interface pressure drop}} + \underbrace{x\Delta P_V}_{\text{vapor pressure drop}} \tag{25}$$

3.2. Development of improved model

The two-phase frictional pressure drop is the sum of liquid pressure drop, vapor pressure drop and interface pressure drop. The liquid and vapor pressure drops are predicted using single-phase correlations from the VDI[30], which are given in Supplementary material A. The interface pressure drop is determined by the two-phase slip, which is a function of fluid properties [43]. Lower mass concentration increases the frictional pressure drop of NH_3/H_2O. The increase is mainly

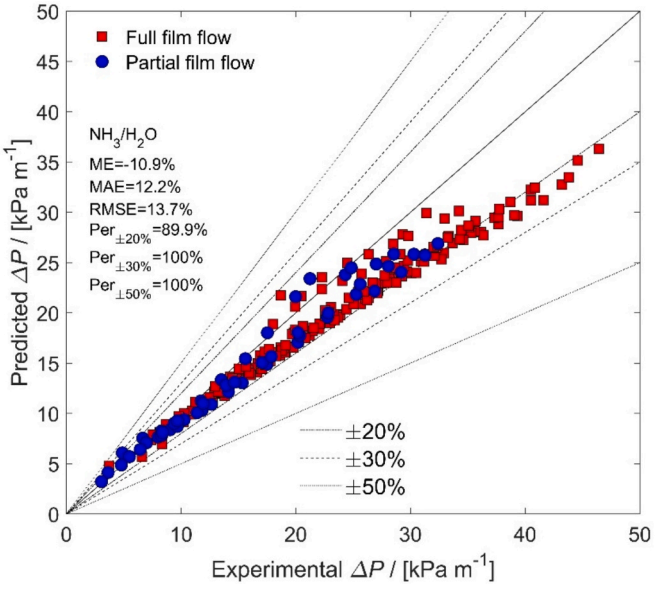

Fig. 17. Comparison of NH_3/H_2O frictional pressure drop with the improved model in Eq. (26).

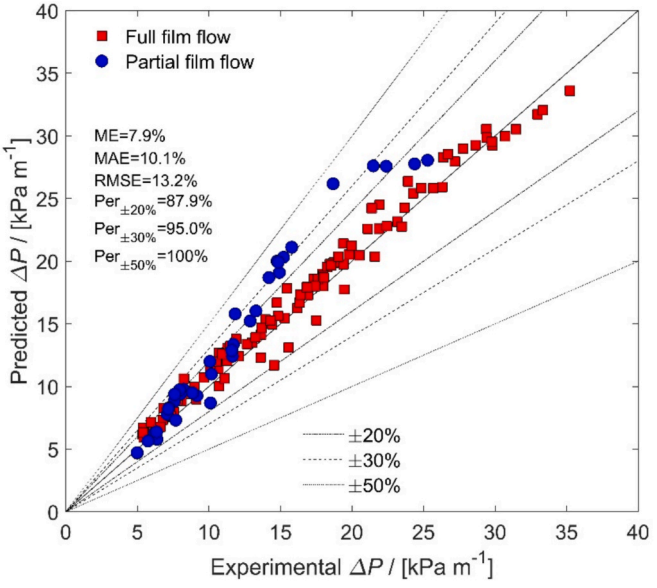

Fig. 18. Comparison of NH_3 frictional pressure drop with the improved model in Eq. (26).

contributed by interface pressure drop. Lower mass concentration increases the two-phase density ratio and viscosity, and the interface pressure drop is aggravated. The model is improved using the reduced pressure and is given in Eq.(26). The reduced pressure indicates the influence of density, viscosity and surface tension. Lower reduced pressure increases the shear force.

$$\Delta P_{TP} = \underbrace{\Delta P_L}_{\text{liqud pressure drop}} + \underbrace{2e^{0.035/P_{re}}\sqrt{\Delta P_L \Delta P_V}}_{\text{interface pressure drop}} + \underbrace{x\Delta P_V}_{\text{vapor pressure drop}} \quad (26)$$

The experimental data are compared with the improved model in Fig. 17. All the experimental data are predicted within ± 30 %. The MAE is 12.2 %, while the RMSE is 13.7 %. The deviations are more noticeable for large frictional pressure drop of full film flow. A unified model is used for full film flow and partial film flow since both flow patterns show similar separated flow characteristics. The liquid film breaks up for partial film flow, whose interface pressure drop is slightly smaller than that of full film flow. The improved model is also validated with the experimental data of pure NH_3, which is shown in Fig. 18. The MAE and RMSE are 10.1 % and 13.2 %, respectively. Several experimental data for partial film flow are over-predicted. The improved model applies to pure NH_3 and high-concentration NH_3/H_2O.

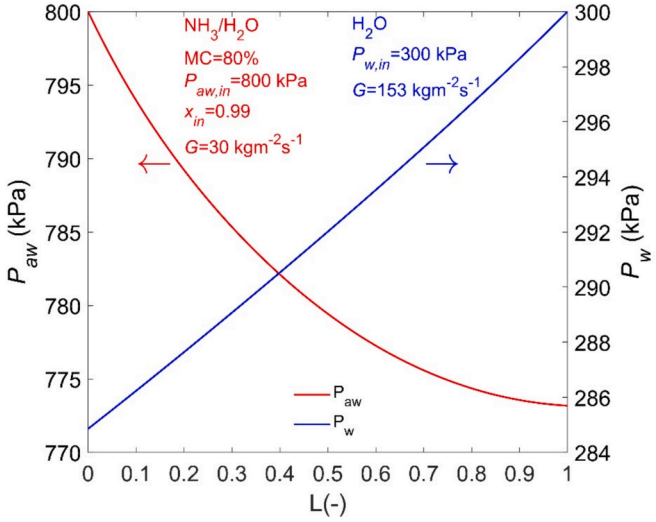

Fig. 19. Pressure profiles of NH_3/H_2O and cooling water along the non-dimensional heat exchanger length.

3.3. Analysis of frictional pressure drop

In Section 2.5.2, the complete condensation is analyzed assuming constant operating pressure. To validate the assumption, the frictional pressure drop is predicted using Eq. (26), which is shown in Fig. 19. The total pressure drop is 26.8 kPa for the two-phase flow. The corresponding temperature change of the bubble point is about 1 K, resulting into the deviation of heat transfer rate for 3.7 % by neglecting the frictional pressure drop. The influence on heat and mass transfer is minor. It is reasonable to assume constant operating pressure and calculate the frictional pressure drop separately. It seems necessary to solve the heat transfer and frictional pressure drop simultaneously for larger mass fluxes or lower pressure. In Fig. 19, the pressure of NH_3/H_2O decreases sharply close to the inlet, where the vapor quality is high. The decrease is gradual close to the outlet. The pressure of cooling water is also given, which changes linearly along the heat exchanger. The total pressure drop is 15.1 kPa and has a negligible effect on the water fluid properties.

4. Discussion of combined models

The heat transfer deterioration of mixture condensation is not constant. The characterization of temperature glide gives insight into the heat transfer deterioration[48]. As shown in Fig. 1, dT/dh depends on the vapor quality for zeotropic mixtures with large temperature glide. It is necessary to interpret the local value of dT/dh instead of average $\Delta T_{LV}/\Delta h_{LV}$. The variation of dT/dh helps to explain the large mass transfer resistance at high vapor qualities.

H_2O (the less volatile component) condenses first from the vapor phase to the liquid phase. NH_3 (the volatile component) accumulates in the vapor, and the NH_3 concentration increases during the condensation. NH_3 has a higher concentration at the vapor interface than the vapor bulk, which reduces the interfacial temperature. It takes place for high vapor qualities. The equilibrium model cannot predict the concentration difference, underestimating the heat transfer. The non-equilibrium model overcomes this drawback and is indispensable.

Temperature difference and concentration difference drive the phase change. The concentrations at the vapor interface and vapor bulk cannot be higher than 100 %, and thus the concentrations become identical as NH_3 accumulates. In this case, the phase change is only driven by the temperature difference. According to Eq. (14), the total condensing flux indicated by the concentration difference is zero, which is incompatible with that in Eq. (18) indicated by the temperature difference. The non-equilibrium model is unsuitable when the concentration difference diminishes, and the equilibrium model complements. This is the condition for high concentration NH_3/H_2O of low vapor qualities.

Both equilibrium and non-equilibrium models are necessary to capture a wide range of concentration difference, which mainly depends on the fluid types and bulk concentrations. Macdonald and Garimella [29] proposed to choose between equilibrium and non-equilibrium models based on $\Delta T_{LV}/\Delta h_{LV}$. Moreover, considering the sharp slope of the temperature glide shown in Fig. 1, the transition of the non-equilibrium and equilibrium models is intrinsic for complete condensation. Webb et al. [47] suggested to distinguish between non-equilibrium and equilibrium models referring to Lewis number, *Le,* which is the ratio of thermal diffusivity to mass diffusivity. According to this analysis, the transition of the models depends on the concentration gradient of vapor and is independent of *Le*.

The total heat transfer of condensation includes the latent heat and sensible heat. The total heat transfer is driven by the temperature difference between the interface and cold wall for both models. The interface is at saturated condition. The mass transfer of the equilibrium model is not calculated directly, but is indicated by additional heat transfer resistance. The interfacial concentration is the same as the overall bulk concentration. The non-equilibrium model calculates the concentration gradient of vapor. The interfacial concentration is different from the overall bulk concentration.

The model is based on high-concentration NH_3/H_2O in PHEs. The additional heat transfer resistance in Eqs. (9)-(12) is originally derived from experimental data[43]. The model is further validated and analyzed in Section 2.5 [44]. The applicability range is presented in Table 7. Since the model depends on the flow patterns in PHEs, it is recommended for separated flow with noticeable shear force. As discussed in our previous work[40,42], the choice of frictional pressure drop model depends on the two-phase density ratio, but is independent of mass transfer resistance. Eq. (26) applies to pure fluids and mixtures of large two-phase density ratios.

As presented in Supplementary material A, the geometrical parameters are involved in the single-phase correlations of heat transfer and frictional pressure drop. The single-phase heat transfer is used for the condensation correlation with the form of a two-phase multiplier. The two-phase frictional pressure drop is composed of the values of single-phase. The model is anticipated to cover most commercial PHEs with hydraulic diameters and chevron angles spanning the range of 2–6 mm and 25°-70°, respectively[40].

High-concentration NH_3/H_2O is the working fluid of the Kalina cycle. The vapor quality range is in low and intermediate values [43]. According to the phase change mechanism, the condensation HTCs approach liquid phase HTCs as the vapor quality becomes zero. However, the transition of high vapor quality condensation to vapor heat transfer is not fully understood. It seems to be a combination of dropwise condensation and convective condensation [1,34,51]. Because H_2O condenses preferentially, the temperature glide changes sharply for high vapor qualities. The vapor mass transfer resistance is significant. The condensation correlations should be used with concern for high vapor qualities. The industrial applications use a large number of channels to increase the capacity, so that the flow maldistribution becomes noticeable. A flow distribution model is required to be coupled with the heat and mass transfer prediction. Additionally, when used for absorption energy storage, the heat and mass transfer is transient, and the time-dependent prediction is necessary [35].

Table 7
Applicability range of the combined model.

NH_3 *MCs*	*G*	*x*	*P*
–	$kgm^{-2}s^{-1}$	–	kPa
≥57 %	18–86	0.01–0.99	580—800

5. Conclusions

In this paper, the condensation of high-concentration NH_3/H_2O is analyzed by discussing the transition from the non-equilibrium model to the equilibrium model. A strategy is suggested to implement the combined method. The main conclusions are below:

- Two-phase NH_3/H_2O is divided into the approximately-linear temperature glide region and non-linear temperature glide region. The non-equilibrium model applies to the non-linear temperature glide region, while the equilibrium model is generally applicable to the approximately-linear temperature glide region. The inlet conditions of vapor and liquid are decisive to apply the equilibrium assumption.
- An equilibrium model is derived from the experimental data presented in a previous paper by the authors [43]. It is based on the transition from convective condensation to gravity-controlled condensation. The additional heat transfer resistance is quantified considering the stratification effect. A non-equilibrium model is developed using the condensation HTCs of the equilibrium model. The heat and mass transfer of vapor are calculated to determine the interface concentration.
- Both equilibrium and non-equilibrium models are necessary for the condensation of zeotropic mixtures spanning a wide range of vapor qualities. The equilibrium model cannot predict the concentration difference between the vapor interface and vapor bulk. As the vapor concentration difference becomes zero, the phase change is only driven by the temperature difference, and the mass transfer equation should be excluded. For the low vapor qualities of mixtures with large temperature glide, the interface concentration approaches equilibrium concentration, and thus the equilibrium model is bridged with the non-equilibrium model.
- A frictional pressure drop model is proposed for separated flow, which is applicable to pure NH_3 and high-concentration NH_3/H_2O. Lower mass concentration increases the interface pressure drop because of the larger two-phase density ratio and viscosity. The sensitivity to mass concentration is quantified.

Declaration of competing interest

The authors declare the following financial interests/personal relationships which may be considered as potential competing interests: Xuan Tao reports financial support was provided by Zhejiang Provincial Natural Science Foundation of China. Bo Wang reports financial support was provided by National Natural Science Foundation of China. If there are other authors, they declare that they have no known competing financial interests or personal relationships that could have appeared to influence the work reported in this paper.

Acknowledgements

This research was supported by the Baima Lake Laboratory Joint Funds of the Zhejiang Provincial Natural Science Foundation of China under Grant No. LBMHY24E060008 and National Natural Science Foundation of China under Grant No. 52476020.

Appendix A. Supplementary data

Supplementary data to this article can be found online at https://doi.org/10.1016/j.applthermaleng.2025.128315.

Data availability

Data will be made available on request.

References

[1] E. Aminian, M. Kamali, E. Vatanjoo, H. Saffari, Theoretical analysis on condensation heat transfer on microstructured hybrid hydrophobic-hydrophilic tube, Heat Mass Transfer 58 (2022) 1207–1221.

[2] M. Aminyavari, M. Aprile, T. Toppi, S. Garone, M. Motta, A detailed study on simultaneous heat and mass transfer in an in-tube vertical falling film absorber, Int. J. Refrig 80 (2017) 37–51.

[3] M. Aminyavari, M. Aprile, L. Pistocchini, M. Motta, Modelling and experimental validation of an in-tube vertical falling film absorber with counter flow arrangement of solution and gas, Int. J. Refrig 100 (2019) 72–82.

[4] K.J. Bell, M.A. Ghaly, An approximate generalized design method for multicomponent/partial condenser, AIChE., Symp 39 (1973) 72–79.

[5] J. Cerezo, M. Bourouis, M. Vallès, A. Coronas, R. Best, Experimental study of an ammonia–water bubble absorber using a plate heat exchanger for absorption refrigeration machines, Appl. Therm. Eng. 29 (2009) 1005–1011.

[6] J. Cerezo, R. Best, M. Bourouis, A. Coronas, Comparison of numerical and experimental performance criteria of an ammonia–water bubble absorber using plate heat exchangers, Int. J. Heat Mass Transf. 53 (2010) 3379–3386.

[7] S. Chandrasekaran, M. Hughes, G. Kini, S. Garimella, A microchannel shell-and-tube absorber for ammonia-water absorption, Appl. Therm. Eng. 185 (2021) 116321.

[8] T.H. Chilton, A.P. Colburn, Mass transfer (absorption) coefficients prediction from data on heat transfer and fluid friction, Ind. Eng. Chem. 26 (1934) 1183–1187.

[9] D. Chisholm, A theoretical basis for the Lockhart-Martinelli correlation for two-phase flow, Int. J. Heat Mass Transf. 10 (1967) 1767–1778.

[10] A.P. Colburn, T.B. Drew, The condensation of mixed vapors, Trans. Am. Inst. Chem. Eng. 33 (1937) 197–212.

[11] M. Conde Engineering Thermophysical properties of ammonia-water mixtures for the industrial design of absorption refrigeration equipment 2006 Zurich.

[12] D. Del Col, A. Cavallini, J.R. Thome, Condensation of zeotropic mixtures in horizontal tubes: new simplified heat transfer model based on flow regimes, J. Heat Trans. 127 (2005) 221–230.

[13] H. Deng, M. Rossato, M. Fernandino, D. Del Col, A new simplified model for condensation heat transfer of zeotropic mixtures inside horizontal tubes, Appl. Therm. Eng. 153 (2019) 779–790.

[14] P. Dou, T. Jia, P. Chu, Y. Dai, Theoretical analysis of single/double-stage NH_3-H_2O long-term resorption energy storage cycle, Appl. Therm. Eng. 274 (2025) 126579.

[15] B.M. Fronk, S. Garimella, In-tube condensation of zeotropic fluid mixtures: a review, Int. J. Refrig 36 (2013) 534–561.

[16] B.M. Fronk, S. Garimella, Condensation of ammonia and high-temperature-glide ammonia/water zeotropic mixtures in minichannels–Part I: Measurements, Int. J. Heat Mass Transf. 101 (2016) 1343–1356.

[17] B.M. Fronk, S. Garimella, Condensation of ammonia and high-temperature-glide ammonia/water zeotropic mixtures in minichannels–Part II: Heat transfer models, Int. J. Heat Mass Transf. 101 (2016) 1357–1373.

[18] S. Huang, R. Zhou, S. Li, R. Gu, S. Gao, H. Guo, W. Jiang, Y. Li, Experimental study on the enhancement effect of ultrasonic oscillation on an ammonia-water falling film absorber, Appl. Therm. Eng. 263 (2025) 125351.

[19] D.X. Jin, J.T. Kwon, M.H. Kim, Prediction of in-tube condensation heat transfer characteristics of binary refrigerant mixtures, Int. J. Refrig 26 (2003) 593–600.

[20] C.W. Jung, S.S. An, Y.T. Kang, Thermal performance estimation of ammonia-water plate bubble absorbers for compression/absorption hybrid heat pump application, Energy 75 (2014) 371–378.

[21] Y.T. Kang, R.N. Christensen, T. Kashiwagi, F. Ziegler, Ammonia-water bubble absorber with a plate heat exchanger/Discussion, ASHRAE Trans. 104 (1998) 1565–1576.

[22] Y.T. Kang, A. Akisawa, T. Kashiwagi, Analytical investigation of two different absorption modes: falling film and bubble types, Int. J. Refrig 23 (2000) 430–443.

[23] J.D. Killion, S. Garimella, A critical review of models of coupled heat and mass transfer in falling-film absorption, Int. J. Refrig 24 (2001) 755–797.

[24] K.B. Lee, B.H. Chun, J.C. Lee, J.C. Hyun, S.H. Kim, Comparison of heat and mass transfer in falling film and bubble absorbers of ammonia-water, Exp. Heat Transfer 15 (2002) 191–205.

[25] E.W. Lemmon I.H. Bell M.L. Huber M.O. McLinden NIST Standard Reference Database 23: Reference Fluid Thermodynamic and Transport Properties-REFPROP, Version 10.0, National Institute of Standards and Technology, Standard Reference Data Program 2018 Gaithersburg.

[26] Y. Li, Y. Li, H. Zhang, W. Zheng, J. Wang, Thermodynamic analysis of a hybrid ammonia-water refrigeration cycle with low-temperature solar heat, Appl. Therm. Eng. 253 (2024) 123791.

[27] Z. Li, P. Zhang, K. Guan, R.R. Gonzales, T. Ishigami, M. Xue, T. Yoshioka, H. Matsuyama, An experimental study on recovering and concentrating ammonia by sweep gas membrane distillation, Process Saf. Environ. 171 (2023) 555–560.

[28] R.W. Lockhart, R.C. Martinelli, Proposed correlation of data for isothermal two-phase, two-component flow in pipes, Chem. Eng. Prog. 45 (1949) 39–48.

[29] M. Macdonald, S. Garimella, Modeling of in-tube condensation of zeotropic mixtures, J. Heat Trans. 138 (2016) 091502.

[30] H. Martin, Pressure drop and heat transfer in plate heat exchangers, in: P. Stephan, H. Martin, S. Kabelac, D. Mewes, M. Kind, K. Schaber (Eds.), VDI Heat Atlas, 2nd Edition, Springer, Dusseldorf, 2010, pp. 1516–1521.

[31] W.J. Minkowycz, E.M. Sparrow, Condensation heat transfer in the presence of noncondensables, interfacial resistance, superheating, variable properties, and diffusion, Int. J. Heat Mass Transf. 9 (1966) 1125–1144.

[32] J. Pan, Q. Cao, J. Zhang, M. Li, L. Tang, R. Li, Design and optimization of a combined supercritical CO2 recompression Brayton/Kalina cycle by using solar energy and LNG cold energy, Appl. Therm. Eng. 247 (2024) 123106.

[33] B.C. Price, K.J. Bell. Design of binary vapor condensers using the Colburn-Drew equations, Oklahoma State University, 1973.

[34] S. Shahlaei, E. Aminian, M. Kamali, H. Saffari, Experimental Study of Condensation Heat transfer on Thermally improved Hybrid Teflon-Copper Vertically Patterned Surfaces, Heat Transfer Engineering (2024) 1–19.

[35] T. Shen, D. Lu, Z. Liu, R. Chen, M. Gong, Heat and mass transfer performance analysis of a vertical tubular ammonia/water bubble absorber based on CFD modelling, Appl. Therm. Eng. 252 (2024) 123622.

[36] Shi, L., Absorption of Ammonia-Water and CO2-NH3-H2O Mixture in Mini-Channel Heat Exchangers. Thesis, TU Delft. 2017.

[37] J. Sieres, J. Fernández-Seara, Modeling of simultaneous heat and mass transfer processes in ammonia–water absorption systems from general correlations, Heat Mass Transfer 44 (2007) 113–123.

[38] L. Silver, Gas cooling with aqueous condensation, Trans. Inst. Chem. Eng. 25 (1947) 30–42.

[39] X. Tao, M.P. Nuijten, C.A. Infante Ferreira, Two-phase vertical downward flow in plate heat exchangers: Flow patterns and condensation mechanisms, Int. J. Refrig 85 (2018) 489–510.

[40] X. Tao, C.A. Infante Ferreira, Heat transfer and frictional pressure drop during condensation in plate heat exchangers: Assessment of correlations and a new method, Int. J. Heat Mass Transf. 135 (2019) 996–1012.

[41] X. Tao, E. Dahlgren, M. Leichsenring, C.A. Infante Ferreira, NH_3 condensation in a plate heat exchanger: Experimental investigation on flow patterns, heat transfer and frictional pressure drop, Int. J. Heat Mass Transf. 151 (2020) 119374.

[42] X. Tao, C.A. Infante Ferreira, NH_3 condensation in a plate heat exchanger: Flow pattern based models of heat transfer and frictional pressure drop, Int. J. Heat Mass Transf. 154 (2020) 119774.

[43] X. Tao, Y.W. Shen, B. Wang, C.A. Infante Ferreira, Condensation of NH_3/H_2O with mass concentrations of 80%-96%: Experimental study in a plate heat exchanger, Int. J. Refrig 151 (2023) 253–266.

[44] D. Triché, S. Bonnot, M. Perier-Muzet, F. Boudéhenn, H. Demasles, N. Caney, Experimental and numerical study of a falling film absorber in an ammonia-water absorption chiller, Int. J. Heat Mass Transf. 111 (2017) 374–385.

[45] D.M. van de Bor, C. Vasilescu, C.A. Infante Ferreira, Experimental investigation of heat transfer and pressure drop characteristics of ammonia–water in a mini-channel annulus, Exp. Therm Fluid Sci. 61 (2015) 177–186.

[46] K. Wang, J. Teng, X. Wei, S. Zhu, S. Fang, L. Qiu, Experimental investigation of thermal and conversion performance of catalysts-filled plate-fin heat exchangers for hydrogen liquefaction, Int. J. Hydrogen Energ. 110 (2024) 814–825.

[47] D.R. Webb, M. Fahrner, R. Schwaab, The relationship between the Colburn and silver methods of condenser design, Int. J. Heat Mass Transf. 39 (1996) 3147–3156.

[48] S. Yan, X. Dong, F. Nie, M. Gong, A new heat transfer model based on non-equilibrium film theory for annular flow condensation of binary zeotropic mixtures, Int. J. Heat Mass Transf. 205 (2023) 123899.

[49] A. Zarei, S. Zaboli, M. Babaie Rabiee, Energy and exergy analysis of a high-efficiency multi-evaporator absorption refrigeration system with integrated ejectors and compression cooling system, Appl. Therm. Eng. 267 (2025) 125753.

[50] Y. Zhang, L. Jia, C. Dang, Z. Qi, The mass transfer characteristics of R134a/R245fa during stratified flow condensation in rectangular channel, Int. J. Heat Mass Transf. 195 (2022) 123189.

[51] A. Zolfaghari, E. Aminian, H. Saffari, Numerical investigation on entropy generation in the dropwise condensation inside an inclined pipe, Heat Transf. 51 (2022) 551–577.